

Supervised Learning and Model Analysis with Compositional Data

Shimeng Huang¹, Elisabeth Ailer², Niki Kilbertus^{2,3}, and Niklas Pfister¹

¹Department of Mathematical Sciences, University of Copenhagen, Copenhagen, Denmark

²Helmholtz Munich, Munich, Germany

³Technical University of Munich, Munich, Germany

May 17, 2022

Abstract

The compositionality and sparsity of high-throughput sequencing data poses a challenge for regression and classification. However, in microbiome research in particular, conditional modeling is an essential tool to investigate relationships between phenotypes and the microbiome. Existing techniques are often inadequate: they either rely on extensions of the linear log-contrast model (which adjusts for compositionality, but is often unable to capture useful signals), or they are based on black-box machine learning methods (which may capture useful signals, but ignore compositionality in downstream analyses).

We propose **KernelBiome**, a kernel-based nonparametric regression and classification framework for compositional data. It is tailored to sparse compositional data and is able to incorporate prior knowledge, such as phylogenetic structure. **KernelBiome** captures complex signals, including in the zero-structure, while automatically adapting model complexity. We demonstrate on par or improved predictive performance compared with state-of-the-art machine learning methods. Additionally, our framework provides two key advantages: (i) We propose two novel quantities to interpret contributions of individual components and prove that they consistently estimate average perturbation effects of the conditional mean, extending the interpretability of linear log-contrast models to non-parametric models. (ii) We show that the connection between kernels and distances aids interpretability and provides a data-driven embedding that can augment further analysis. Finally, we apply the **KernelBiome** framework to two public microbiome studies and illustrate the proposed model analysis. **KernelBiome** is available as an open-source Python package at <https://github.com/shimenghuang/KernelBiome>.

1 Introduction

Compositional data, that is, measurements of parts of a whole, are common in many scientific disciplines. For example, mineral compositions in geology (Buccianti et al., 2006), element concentrations in chemistry (Pesenson et al., 2015), species compositions in ecology (Jackson, 1997) and more recently high-throughput sequencing reads in microbiome science (Li, 2015). Mathematically, any p -dimensional composition—by appropriate normalization—can be represented as a point on the simplex

$$\mathbb{S}^{p-1} := \{x \in [0, 1]^p \mid \sum_{j=1}^p x^j = 1\}.$$

This complicates the statistical analysis, because the sum-to-one constraint of the simplex induces non-trivial dependencies between the components that may lead to false conclusions, if not appropriately taken into account.

The statistics community has developed a substantial collection of parametric analysis techniques to account for the simplex-structure. The most basic and often employed parametric model on the simplex is the family of Dirichlet distributions. However, as pointed out already by Aitchison (1982), Dirichlet distributions cannot capture non-trivial dependence structures between the composition components and are thus too restrictive. Aitchison (1982) therefore introduced the *log-ratio* approach. It generates a family of distributions by projecting multivariate normal distributions into \mathbb{S}^{p-1} via an appropriate log-ratio transformation (e.g., the additive log-ratio, centered log-ratio (Aitchison, 1982), or isometric log-ratio (Egozcue et al., 2003)). The resulting family of distributions results in parametric models on the simplex that are rich enough to capture non-trivial dependencies between the components (i.e., beyond those induced by the sum-to-one constraint). The log-ratio approach has been extended and adapted to a range of statistical problems (e.g., Aitchison, 1985; Tsagris et al., 2011; Aitchison, 1983; Aitchison and Greenacre, 2002; Friedman and Alm, 2012).

For supervised learning tasks the log-ratio approach leads to the *log-contrast model* (Aitchison and Bacon-Shone, 1984), which can be seen as an extension of the linear regression model to the simplex. An attractive property of the log-contrast model is that its coefficients quantify the effect of a multiplicative perturbation (i.e., fractionally increasing one component while adjusting the others) on the response. While several extensions of the log-contrast model exist (e.g., Lin et al., 2014; Shi et al., 2016; Simpson et al., 2021; Ailer et al., 2021), its parametric approach to supervised learning has two major shortcomings that become particularly severe when applied to high-dimensional and zero-inflated high-throughput sequencing data (Tsilimigras and Fodor, 2016; Gloor et al., 2017). Firstly, since the logarithm is not defined at zero, the log-contrast model does not directly apply. A common fix is to add so-called pseudo-counts, a small non-zero constant, to all (zero) entries (Kaul et al., 2017; Lin and Peddada, 2020). More sophisticated replacement methods exist as well (e.g., Martín-

Fernández et al., 2003; Fernandes et al., 2013), however, they often rely on an understanding of the nature of the zeros (e.g., whether they are structural or random), which is typically not available in practice and difficult to estimate. In any case, the downstream analysis will strongly depend on the selected zero imputation scheme. Secondly, the relationships between individual components (e.g., species) and the response are generally complex. For example, in human microbiome settings, a health outcome may depend on interactions or on the presence or absence of species. Both signal types cannot be captured by the linear structure of the log-contrast model.

In this work, we propose to solve the supervised learning task using a nonparametric approach based on kernels, which is able to handle complex signals and avoid arbitrary zero-imputation. To be of use in biological applications, there are two components to a supervised analysis: (i) estimating a predictive model that accurately captures the signal in the data and (ii) extracting meaningful and interpretable information from the estimated model. For (i), it has been shown in recent years that modern machine learning methods are capable of creating highly predictive models by using microbiome data as covariates and phenotypes as responses (e.g., Knight et al., 2018; Zhou and Gallins, 2019; Cammarota et al., 2020). In particular, several approaches have been proposed where kernels are used to incorporate prior information (Chen and Li, 2013; Randolph et al., 2018) or as a way to utilize the compositional structure (Ramon et al., 2021; Di Marzio et al., 2015; Tsagris and Athineou, 2021). Part (ii) is related to the fields of explainable AI (Samek et al., 2019) and interpretable machine learning (Molnar, 2020), which focus on extracting information from predictive models. These types of approaches have also received growing attention in the context of microbiome data (Gou et al., 2021; Ruaud et al., 2022; Topçuoğlu et al., 2020). However, to the best of our knowledge, none of these procedures have been adjusted to account for the compositional structure. As we show in Section 2.1, not accounting for the compositionality may invalidate the results.

Our proposed **KernelBiome** framework, see Figure 1, addresses both (i) and (ii). For (i), it provides a data-driven model selection procedure for regression and classification based on a large class of kernels targeted to different aspects of the simplex structure. This leads to models that are flexible in capturing various types of signals and contains the log-contrast model as a special case. Moreover, similarities between components, for example phylogenetic similarity between taxa in ecology applications, can be easily integrated into our framework encoded as a weight matrix resulting in weighted kernels. For (ii), **KernelBiome** provides two ways of analyzing the estimated model. Firstly, we introduce two novel measures for interpreting the effects of individual features that explicitly take the compositionality into account and prove that these can be consistently estimated. Secondly, we build on known connections between kernels and distance measures to advocate for using the kernel embedding from the estimated model to create visualizations and perform follow-up distance-based analyses that respect the compositionality. Finally, we highlight a connection between distances and diversity, which provide a new perspective on commonly used diversity measures.

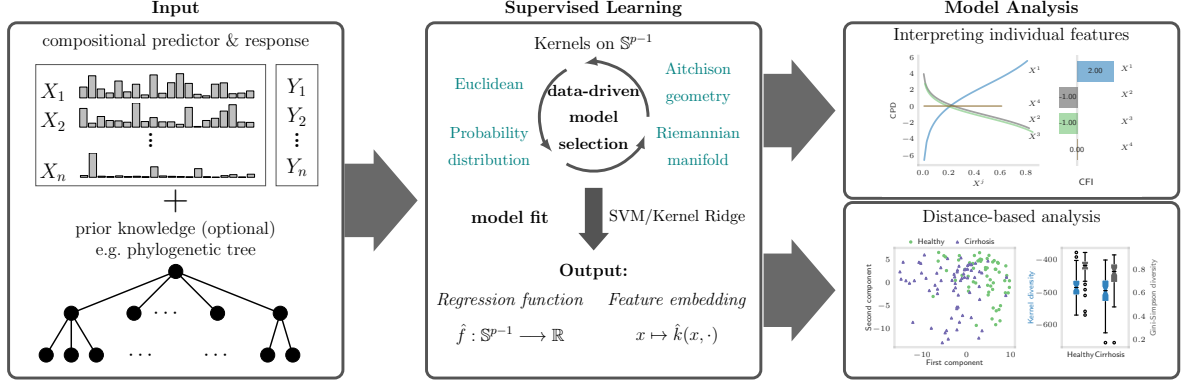


Figure 1: Overview of the **KernelBiome** framework. The starting point is a paired dataset with a compositional predictor X and a response Y and optional prior knowledge on the relation between components in the compositions (e.g., via a phylogenetic tree). We then propose to select a model among a large class of kernels which best fits the data. This results in an estimated model and embedding. Finally, these can be analyze while accounting for the compositional structure in the data.

The paper is structured as follows. In Section 2, we introduce the supervised learning task, define two measures to analyze effects of perturbing individual components (Section 2.1), give a short introduction to kernel methods and how to apply our methodology for regression and classification (Section 2.2), and present the full **KernelBiome** framework including model selection and model analysis (Section 2.3). Model analysis includes assessing diversity measures and dimensionality reduction with appropriate visualizations. We then illustrate the full functionality of **KernelBiome** in the experiments in Section 3. Finally, we conclude with a discussion in Section 4.

2 Methods

We consider the setting in which we observe n independent and identically distributed (i.i.d.) observations $(X_1, Y_1), \dots, (X_n, Y_n)$ of a random variable (X, Y) with $X \in \mathbb{S}^{p-1}$ a compositional predictor and $Y \in \mathbb{R}$ a real-valued response variable (by which we include categorical responses). Supervised learning attempts to learn a relationship between the response Y and the dependent predictors X . In this work, we focus on conditional mean relationships. More specifically, we are interested in estimating (a version of) the conditional mean of Y , that is, the function

$$f^*: x \mapsto \mathbb{E}[Y \mid X = x]. \quad (1)$$

Throughout this work we assume that $f^* \in \mathcal{F} \subseteq \{f \mid f: \mathbb{S}^{p-1} \rightarrow \mathbb{R}\}$, where \mathcal{F} is a function class determined by the regression (or classification) procedure.

While estimating and analyzing the conditional mean is well established for predictors in Euclidean space, there are two factors that complicate the analysis when the predictors are

compositional. (i) While it is possible to directly apply most standard regression procedures designed for $X \in \mathbb{R}$ also for $X \in \mathbb{S}^{p-1}$, it turns out that many approaches are ill-suited to approximate functions on the simplex. (ii) Even if one accurately estimates the conditional mean function f^* , the simplex constraint complicates any direct assessment of the influence and importance of individual components of the compositional predictor. In this work, we address both of these issues and propose a general nonparametric framework for regression and classification analysis for compositional data.

2.1 Interpreting individual features

Our goal when estimating the conditional mean f^* given in (1) is to gain insight into the relationship between the response Y and predictors X . For example, when fitting a log-contrast model (see Example 2.1 below), the estimated coefficients provide a useful tool to generate hypotheses about which features affect the response and thereby inform follow-up experiments. For more complex models, such as the nonparametric kernel methods proposed in this work, direct interpretation of a fitted model \hat{f} is difficult. Two widely applicable methods due to Friedman (2001) are the following: (i) Relative influence, which assigns each coordinate j a scalar influence value given by the expected partial derivative $\mathbb{E}[\frac{d}{dx_j} \hat{f}(X)]$ and (ii) partial dependence plots, which are constructed by plotting, for each coordinate j , the function $z \mapsto \mathbb{E}[\hat{f}(X^1, \dots, X^{j-1}, z, X^{j+1}, \dots, X^p)]$. As argued for example by Kumar et al. (2020) and Hooker et al. (2021), care is needed in applying and interpreting feature-wise influence metrics as they may rely on the fitted model extrapolating beyond the sample support. In Appendix D.2, we illustrate that this indeed happens naturally on the simplex based on two examples in Appendix D.2. We therefore need influence measures that incorporate the simplex constraint.

To this end, we define two coordinate-wise perturbations of a composition. For any $j \in \{1, \dots, p\}$, $x \in \mathbb{S}^{p-1}$ and $c \in [0, 1]$, define (i) $\psi_j(x, c) \in \mathbb{S}^{p-1}$ to be the composition resulting from multiplying the j -th component by c and then scaling the entire vector back into the simplex, and (ii) $\phi_j(x, c) \in \mathbb{S}^{p-1}$ to be the composition that consists of fixing the j -th coordinate to c and then rescaling all remaining coordinates such that the resulting vector lies in the simplex. Each perturbation can be seen as a different way of intervening on a single coordinate in a way that preserves the simplex structure. More details are given in Appendix A. Based on the first perturbation, we define the *compositional feature influence* (CFI) for any differentiable function $f : \mathbb{S}^{p-1} \rightarrow \mathbb{R}$ and all coordinates $j \in \{1, \dots, p\}$ by

$$\text{(CFI)} \quad I_f^j := \mathbb{E} \left[\frac{d}{dc} f(\psi_j(X, c)) \Big|_{c=1} \right]. \quad (2)$$

Similarly, we adapt partial dependence plots using the second perturbation. Define the *compositional feature dependence* (CPD) for any function $f : \mathbb{S}^{p-1} \rightarrow \mathbb{R}$ and all coordinates

$j \in \{1, \dots, p\}$ by

$$(\text{CPD}) \quad S_f^j : z \mapsto \mathbb{E}[f(\phi_j(X, z))] - \mathbb{E}[f(X)]. \quad (3)$$

In practice, we can compute Monte Carlo estimates of both quantities by replacing expectations with empirical means. We denote the corresponding estimators by \hat{I}_f^j and \hat{S}_f^j , respectively (see Appendix A for details).

To gain intuition, let us apply CFI and CPD to the log-contrast model. That is, consider $f : x \mapsto \beta^T \log(x)$ with $\sum_{j=1}^p \beta_j = 0$. In that case the CFI and CPD have the following explicit representation.

Proposition 2.1 (CFI and CPD in the log-contrast model). Let $f : x \mapsto \beta^T \log(x)$ with $\sum_{j=1}^p \beta_j = 0$, then the CFI and CPD are given by

$$I_f^j = \beta_j \quad \text{and} \quad S_f^j : z \mapsto \beta_j \log\left(\frac{z^j}{1-z^j}\right) + c,$$

respectively, where $c \in \mathbb{R}$ is a constant depending on the distribution of X but not on z and satisfies $c = 0$ if $\beta_j = 0$.

A proof is given in Appendix F.1. The proposition shows that the CFI and CPD can be seen as generalizations of the β -coefficients in the log-contrast model. Let us provide a specific example of CFI and CPD in a log-contrast model.

Example 2.1 (CFI and CPD in a log-contrast model). Consider a log-contrast model with

$$f : x \mapsto 2 \log(x^1) - \log(x^2) - \log(x^3).$$

The CFI and CPD for the true function f estimated based on $n = 100$ i.i.d. compositional log-normal samples is shown in Figure 2.

The following theorem highlights the usefulness of the CFI and CPD by establishing when they can be consistently estimated from data.

Theorem 2.1 (Consistency). Assume \hat{f}_n is an estimator of the conditional mean f^* given in (1) based on $(X_1, Y_1), \dots, (X_n, Y_n)$ i.i.d.. Then the following two statements hold.

- (i) If $\frac{1}{n} \sum_{i=1}^n \|\nabla \hat{f}_n(X_i) - \nabla f^*(X_i)\|_2 \xrightarrow{P} 0$ as $n \rightarrow \infty$ and $\mathbb{E}[(\nabla f^*(X_i))^2] < \infty$, then it holds for all $j \in \{1, \dots, p\}$ that

$$\hat{I}_{\hat{f}_n}^j \xrightarrow{P} I_{f^*}^j \quad \text{as } n \rightarrow \infty.$$

- (ii) If $\sup_{x \in \text{supp}(X)} |\hat{f}_n(x) - f^*(x)| \xrightarrow{P} 0$ as $n \rightarrow \infty$ and $\text{supp}(X) = \{w / (\sum_j w^j) \mid w \in \text{supp}(X^1) \times \dots \times \text{supp}(X^p)\}$, then it holds for all $j \in \{1, \dots, p\}$ and all $z \in [0, 1]$ with

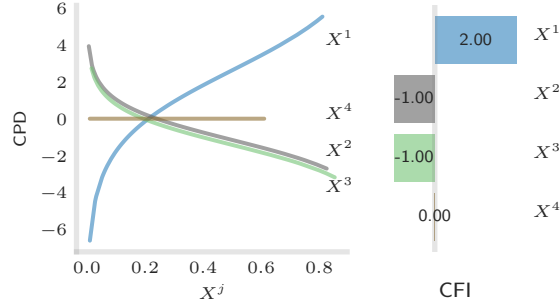


Figure 2: Visualization of the CPD (left) and CFI (right) based on $n = 100$ samples and the true function f . Since $\beta_4 = 0$ in this example the 4-th component has no effect on the value of f resulting in a CFI of zero and a flat CPD. Since we are not estimating f , the CFI values exactly correspond to the β -coefficients in this example.

$z/(1-z) \in \text{supp}(X^j / \sum_{\ell \neq j} X^\ell)$ that

$$\hat{S}_{f_n}^j(z) \xrightarrow{P} S_{f^*}^j(z) \quad \text{as } n \rightarrow \infty.$$

A proof is given in Appendix F.2 and the result is demonstrated on simulated data in Appendix D.1. The theorem shows that the CFI is consistently estimated as long as the derivative of f^* is consistently estimated, which can be ensured for example for the kernel methods discussed in Section 2.2. In contrast, the CPD only requires the function f^* itself to be consistently estimated. The additional assumption on the support ensures that the perturbation ϕ_j used in the CPD remains within the support. If this assumption is not satisfied one needs to ensure that the estimated function extrapolates beyond the sample support. Interpreting the CPD therefore requires caution.

2.2 Kernel methods for compositional data analysis

Kernel methods are a powerful class of nonparametric statistical methods that are particularly useful for data from a non-standard (i.e., non-Euclidean) space \mathcal{X} . The starting point is a symmetric, positive definite¹ function $k : \mathcal{X} \times \mathcal{X} \rightarrow \mathbb{R}$, called kernel. Kernels are often thought to encode a similarity between points in \mathcal{X} , that is, large values of k correspond to points that are similar and small values to points that are less similar. Instead of directly analyzing the data on \mathcal{X} , kernel methods map the data into a well-behaved feature space $\mathcal{H}_k \subseteq \{f \mid f : \mathcal{X} \rightarrow \mathbb{R}\}$, called reproducing kernel Hilbert space (RKHS), whose inner product preserves the similarity structure specified by the kernel.

Here, we consider kernels on the simplex, that is, $\mathcal{X} = \mathbb{S}^{p-1}$. Then, the conditional mean function f^* given in (1) can be estimated by optimizing a loss over \mathcal{H}_k , for an appropriate

¹This means that for all $m \in \mathbb{N}$ and all $x_1, \dots, x_m \in \mathcal{X}$ it holds that $(k(x_i, x_j))_{i,j \in \{1, \dots, m\}}$ is a symmetric positive definite matrix.

kernel k for which \mathcal{H}_k is sufficiently rich, i.e., $f^* \in \mathcal{H}_k$. The representer theorem (e.g., Schölkopf et al., 2002) states that such an optimization over functions in \mathcal{H}_k can be performed efficiently. Formally, it states that the minimizer of a general loss over \mathcal{H}_k of the form

$$\hat{f} = \arg \min_{f \in \mathcal{H}_k} L((Y_1, f(X_1)), \dots, (Y_n, f(X_n))) + \lambda \|f\|_{\mathcal{H}_k}^2,$$

with convex $L : \mathbb{R}^{2n} \rightarrow [0, \infty)$ an arbitrary loss function and $\lambda > 0$ a penalty parameter, has the form $\hat{f}(\cdot) = \sum_{i=1}^n \hat{\alpha}_i k(X_i, \cdot)$ for some $\hat{\alpha} \in \mathbb{R}^n$. This means that instead of optimizing over a potentially infinite-dimensional space \mathcal{H}_k , it is sufficient to optimize over the n -dimensional parameter $\hat{\alpha}$. Depending on the loss function, this allows to construct efficient regression and classification procedures, such as kernel ridge regression and support vector machines (e.g., Schölkopf et al., 2002).

The performance of the kernel approach depends on the choice of kernel. One way of thinking about this choice is to draw a connection between kernels and distances. Any fixed kernel k on \mathcal{X} induces a semi-metric² d on \mathcal{X} defined for all $x, y \in \mathcal{X}$ by

$$d^2(x, y) = k(x, x) + k(y, y) - 2k(x, y). \quad (4)$$

In particular, this corresponds to the distance between the embedded points in the RKHS \mathcal{H}_k . A partial reverse implication is also true. For a particular type of semi-metric d on \mathcal{X} it is possible to construct a kernel k on \mathcal{X} defined for all $x, y \in \mathcal{X}$ by

$$k(x, y) = -\frac{1}{2}d^2(x, y) + \frac{1}{2}d^2(x, x_0) + \frac{1}{2}d^2(x_0, y),$$

where $x_0 \in \mathcal{X}$ is an arbitrary reference point, such that the distance in the corresponding RKHS \mathcal{H}_k is d . We provide a formal overview of the connection between kernels and distances including proofs in Appendix E. This connection has two important implications in the context of this paper. (i) It provides a natural way for constructing kernels based on established distances on the simplex. The intuition being that a distance, which is large for observations with vastly different responses and small otherwise, leads to an informative feature space \mathcal{H}_k . (ii) It motivates using the kernel-induced distance to analyze the data. We discuss this in Section 2.3.2.

2.2.1 Kernels on the simplex

We consider the following four types of kernels on the simplex (see Table 1), each related to different types of distances on the simplex. A full list with all kernels and induced distances is provided in Appendix G.

²A semi-metric d satisfies all properties of a metric, except that $d(x, y) = 0$ does not imply $x = y$. This can happen because a kernel can map two different points in \mathcal{X} to the same point in \mathcal{H}_k .

Euclidean: These are kernels that are constructed by restricting kernels on \mathbb{R}^p to the simplex. Any such restriction immediately guarantees that the restricted kernel is again a kernel. However, the induced distances are not targeted to the simplex and therefore can be unnatural choices. In the `KernelBiome` framework, we have included the linear kernel and the radial basis function (RBF) kernel. The RBF kernel is L^p -universal (e.g., Sriperumbudur et al., 2011) which means that it can approximate any integrable function (in the large sample limit). However, this does not necessarily imply good performance for finite sample sizes.

Aitchison geometry: One way of incorporating the simplex structure is to use the Aitchison geometry. Essentially, this corresponds to mapping points from the interior of the simplex via the centered log-ratio transform into \mathbb{R}^p and then using the Euclidean geometry. This results in the Aitchison kernel for which the induced RKHS is equal to the log-contrast functions. In particular, applying kernel ridge regression with an Aitchison kernel corresponds to fitting a log-contrast model with a penalty on the size of the coefficients. In the `KernelBiome` package, we include the Aitchison kernel and the Aitchison-RBF kernel which combines the Aitchison and RBF kernels. As the centered log-ratio transform is only defined for interior points in the simplex, we add a hyperparameter to the kernels that shift them away from zero. From this perspective, the commonly added pseudo-count constant added to all components becomes a tuneable hyperparameter of our method, rather than a fixed ad-hoc choice during data pre-processing. Thereby, the Aitchison kernels in `KernelBiome` respect the fact that current approaches to zero-replacement or imputation are often not biologically justified, yet may impact predictive performance.

Probability distributions: Another approach to incorporating the simplex structure into the kernel is by viewing points in the simplex as discrete probability distributions. This allows us to make use of the extensive literature on distances between probability distributions to construct kernels. `KernelBiome` includes (i) a parametric class of kernels, which we call generalized-JS, based on generalized Jensen-Shannon distances due to Topsøe (2003), and (ii) a parametric class, which we call Hilbertian, based on the work by Hein and Bousquet (2005). Together they contain many well-established distances such as the total variation, Hellinger, Chi-squared, and Jensen-Shannon distance. All resulting kernels naturally allow for sparse compositions.

Riemannian manifold: Finally, the simplex structure can be incorporated by using a multinomial distribution which has a parameter in the simplex. Lafferty et al. (2005) show that the geometry of multinomial statistical models can be exploited by using kernels based on the heat equation on a Riemannian manifold. The resulting kernel is known as the heat-diffusion kernel and has been observed to work well in settings with many zeros.

Geometry	Kernel	Parameters
Euclidean	linear RBF	none bandwidth σ
Probability distributions	generalized-JS Hilbertian	$a \in [1, \infty], b \in [\frac{1}{2}, a]$ $a \in [1, \infty], b \in [-\infty, -1]$
Aitchison geometry	Aitchison Aitchison-RBF	zero-shift c zero-shift c , bandwidth σ
Riemannian manifold	heat-diffusion	heat parameter t

Table 1: Types of simplex kernels contained in `KernelBiome`.

2.2.2 Including prior information into kernels

All kernels introduced in the previous section (and described in detail in Appendix G) are invariant under permutations of the compositional components. In particular, they do not take into account any relation between the components. In many applications, one may however have prior knowledge about the relation between the components. For example, if the compositional predictor consists of relative abundances of microbial species, information about the genetic relation between different species encoded in a phylogenetic tree may be available. Therefore, we provide the following way to incorporate such relations. Assume the prior information has been expressed as a positive semi-definite weight matrix $W \in \mathbb{R}^{p \times p}$ with non-negative entries (e.g., using the UniFrac-Distance (Lozupone and Knight, 2005) as shown in Appendix B.3), where the ij -th entry corresponds to the strength of the relation between components i and j . We can then incorporate W directly into our kernels. To see how this works, consider the special case where the kernel k can be written as

$$k(x, y) = \sum_{i=1}^p k_0(x^i, y^i) \quad (5)$$

for a positive definite kernel $k_0 : [0, 1] \times [0, 1] \rightarrow \mathbb{R}$. Then, the weighted kernel k_W defined by

$$k_W(x, y) = \sum_{i,j=1}^p W_{i,j} \cdot k_0(x^i, y^j) \quad (6)$$

is positive definite and incorporates the prior information in a natural way. If two components i and j are known to be related (corresponding to large values of $W_{i,j}$), the kernel k_W takes the similarity across these components into account. In Appendix B.2, we show that the probability distribution kernels and the linear kernel can be expressed as in (5) and propose similar weighted versions for the remaining kernels.

2.3 KernelBiome framework

For a given i.i.d. dataset $(X_1, Y_1), \dots, (X_n, Y_n)$, the **KernelBiome** framework (see Figure 1) first runs a data-driven model selection, resulting in an estimated regression function \hat{f} and a specific kernel \hat{k} . Then, the feature influence properties (CFI, CPD) and embedding induced by \hat{k} are analyzed in a way that respects compositionality.

2.3.1 Model selection

Each kernel discussed in Section 2.2.1 captures different aspects of the data, hence their comparative performance depends on the signals encoded in the data. We therefore propose the following data-driven selection procedure, which is based on hierarchical cross-validation (CV):

1. Split the sample into N_{out} subsets. These subsets are used for N_{out} -fold outer CV to select the best kernel and corresponding kernel parameters (e.g., bandwidth for the RBF kernel, see Table 1).
2. Split each subset further into N_{in} subsets. These subsets are used for N_{in} -fold inner CV to select the best hyperparameters for the algorithm (e.g., regularization parameter for kernel ridge regression).
3. Select the best kernel \hat{k} and its kernel parameters based on the average test score of the outer CV.
4. Split the entire dataset into N_{refit} subsets. Perform N_{refit} -fold CV using the best kernel with the best kernel parameters to select the best hyperparameters of the method again.

The final estimator \hat{f} is obtained by refitting the entire dataset using the best kernel type with the best kernel parameters and the best fitting method hyperparameters. The **KernelBiome** package provides default parameter grids for the kernel parameters of each kernel type, but it is also straightforward to specify them by the user.

2.3.2 Model analysis

We propose three different ways to analyze the estimated model.

Compositional feature importance: As discussed in Section 2.1, feature influence methods for \hat{f} developed for functions on \mathbb{R}^p can yield misleading results. Instead, we employ the CPD and CFI to analyze how a single component affects the outcome.

Distance-based analysis: A key advantage of the **KernelBiome** framework is that beyond the estimated function \hat{f} it also outputs the corresponding kernel \hat{k} that resulted in the best fit. As discussed in Section 2.2, this kernel induces a distance on the simplex that is

well-suited to separate observations in the simplex with different Y values. We therefore suggest to utilize this distance to investigate the data further. Essentially, any statistical method based on distances can be applied at this stage. We suggest the following in particular: (i) Use multi-dimensional scaling (MDS), or equivalently kernel PCA, based on the estimated distance \hat{d} . This can be a useful tool to investigate whether certain observations are outliers, or whether additional structure in the data becomes visually apparent, which may be worth investigating. Details are provided in Appendix E.2. (ii) Use clustering, for example k-means clustering, to investigate whether some (groups of) samples are related.

Data-driven diversity: Diversity is a key measure used to describe ecological communities via a scalar summary statistic. In this context, a community can be thought of as a single observation in the simplex and diversity as the variation within the community (α -diversity). There is no universally agreed upon definition and various versions exist, some of which also include, for example, phylogenetic structure (e.g., Leinster and Cobbold, 2012; Chao et al., 2014; Daly et al., 2018).

Kernels on the simplex provide a useful perspective on diversity. Assuming that every point $x \in \mathbb{S}^{p-1}$ corresponds to a single community, it is natural to consider the point $u = (1/p, \dots, 1/p) \in \mathbb{S}^{p-1}$ as being the most diverse community (ignoring potential relationships between components). For any fixed kernel k on the simplex, it is therefore reasonable to define for all $x \in \mathbb{S}^{p-1}$ a corresponding diversity by

$$D^k(x) := -d_k^2(x, u),$$

where d_k is the distance induced by the kernel k .

While such a definition of diversity does not necessarily satisfy all desirable properties for diversities (see e.g., Leinster and Cobbold, 2012), it is (i) symmetric, (ii) has an intuitive interpretation and (iii) is well-behaved when combined with weighted kernels. Connections to established diversities also exist, for example, the linear kernel corresponds to a shifted version of the Gini-Simpson diversity (i.e., $\text{Gini-Simpson}(x) := 1 - \sum_{j=1}^p (x^j)^2 = D^k(x) + \frac{p-2}{p}$). We believe that these data-driven diversities may offer an interesting avenue for future research.

2.3.3 Implementation

The `KernelBiome` framework is implemented as a Python (van Rossum and Drake, 2009) package that takes advantage of the high-performance `JAX` (Bradbury et al., 2018) and `scikit-learn` (Pedregosa et al., 2011) libraries. All kernels introduced are implemented with `JAX`'s just-in-time compilation and automatically leverage accelerators such as GPU and TPU when available.

`KernelBiome` provides fast computation of all kernels and distance metrics listed in Table 1 as well as easy-to-use procedures for model selection and comparison. Additionally, it includes procedures for CPD and CFI estimation, MDS plots, and diversity calculation based on a

fitted model. The framework and extensive examples on how to utilize it are available at <https://github.com/shimenghuang/KernelBiome>.

3 Results

In this section, we evaluate our framework on two microbiome datasets: (i) **Cirrhosis** (Qin et al., 2014) based on a study analyzing the differences in microbial compositions between $n = 130$ healthy and cirrhotic patients, and (ii) **CentalParkSoil** (Ramirez et al., 2014) based on a study analyzing the PH concentration using microbial compositions from $n = 580$ soil samples. For both datasets, we aggregate the microbiome amplicon data to species level, and then perform a pre-screening step to select species with high average abundance and prevalence, resulting in $p = 108$ and $p = 114$ species for the two datasets, respectively (see Appendix C.1).

3.1 State-of-the-art prediction performance

We compare the predictive performance of **KernelBiome** on both microbiome datasets with the following competitors: (i) **Baseline**, a naive baseline that predicts the majority class for classification and the mean for regression, (ii) **SVM-RBF**, a support vector machine with the RBF kernel, (iii) **Lin/Log-L1**, a linear/logistic regression with ℓ^1 -penalty (iv) **LogCont-L1**, a log-contrast regression with ℓ^1 penalty with 1 added as pseudo-count to remove zeros, and (v) **RF**, a random forest. For **SVM-RBF**, **Lin/Log-L1** and **RF** we use the **scikit-learn** implementations (Pedregosa et al., 2011) and choose the hyperparameters (bandwidth, number of trees and all penalty parameters) based on a 5-fold CV. For **LogCont-L1** we use the **c-lasso** package (Simpson et al., 2021) and the default CV scheme to chose the penalty parameter. We apply both an unweighted and weighted version of **KernelBiome**. The weighted version (**KernelBiome-UF**) uses the UniFrac-based weights described in Appendix B.3. In both cases, the default parameter grid and $N_{\text{in}} = 5$, $N_{\text{out}} = 10$ are used.

We compare methods by performing a 50-fold train/test split and recording the predictive performance (accuracy for classification and mean-squared error (MSE) for regression) on each test set shown in Figure 3. On both datasets the unweighted version of **KernelBiome** performs at least as well as all competing methods and on the Cirrhosis dataset **KernelBiome** improves slightly over other approaches. Overall the weighted version performs slightly worse, which may imply that species that are similar in terms of UniFrac-distance may not necessarily have similar relations to the responses (here cirrhosis indicator and PH levels).

On the Cirrhosis dataset **KernelBiome** selected the Aitchison kernel on all but one train/test splits. Since the Aitchison kernel corresponds to the log-contrast model (with the exception of the data-driven choice of zero-imputation), we expected a similar performance of **KernelBiome** and **Lin/Log-L1**. Indeed, in Figure 3, **KernelBiome** only outperforms **Lin/Log-L1** on a few

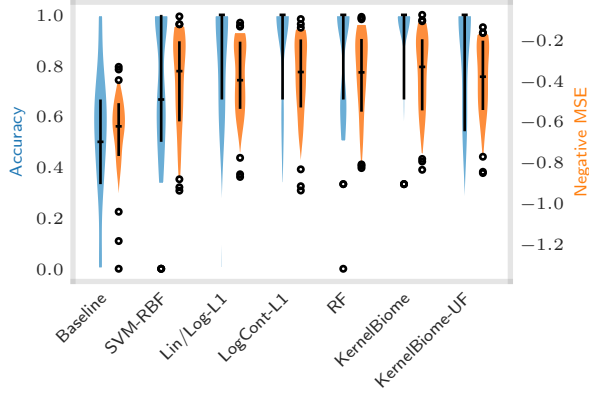


Figure 3: Comparison of predictive performance on Cirrhosis (blue; accuracy) and CentralParkSoil datasets (orange; negative mean squared error) based on a 50-fold train/test split. The score values below 5% and above 95% quantiles are plotted as circles and the inner 90% are used to create the violins. The horizontal bars mark the median and the vertical bars mark the range from 25% to 75% percentile of the scores.

train/test splits, which we attribute to the data-driven zero-imputation. In contrast, on the CentralParkSoil dataset **KernelBiome** selected mostly probability distribution type kernels, leading to a larger model classes. As seen in Figure 3, **KernelBiome** outperforms **Lin/Log-L1** in terms of median negative MSE on this dataset. This illustrates that **KernelBiome** is able to adapt the model complexity to the data.

3.2 CFI reflects prior information

As discussed in Section 2.2.2, it is possible to include prior information into **KernelBiome**. We illustrate this on the Cirrhosis dataset. Assume that the species are indexed from 1 to 108 and that *Veillonella parvula* and *Streptococcus parasanguinis* are the first and second species, respectively. Now, for the sake of illustration, assume that it is biologically true that *Veillonella parvula* and *Streptococcus parasanguinis* have the same functional characteristics, while all other species have unique functional characteristics.³ This information can be included into **KernelBiome** by using the following weight matrix

$$W = \begin{pmatrix} \begin{pmatrix} 0.5 & 0.5 \\ 0.5 & 0.5 \end{pmatrix} & 0 \\ 0 & \text{Id}_{106 \times 106} \end{pmatrix} \in \mathbb{R}_{\geq 0}^{108 \times 108}, \quad (7)$$

where $\text{Id}_{106 \times 106}$ is the 106-dimensional identity matrix. The CFIs computed by applying **KernelBiome** once with W and once without are provided in Figure 4 (left). The species in the plot are sorted according to the unweighted absolute CFIs and *Veillonella parvula* and *Streptococcus parasanguinis* are highlighted with red labels. Without the weighting the two

³This only serves to illustrate the effect of the weighting and is not based on any biological knowledge.

species have different CFI values, while they become almost identical with the weighting. For all other species the weighting only has a small effect. This shows how the prior information is captured in the CFI.

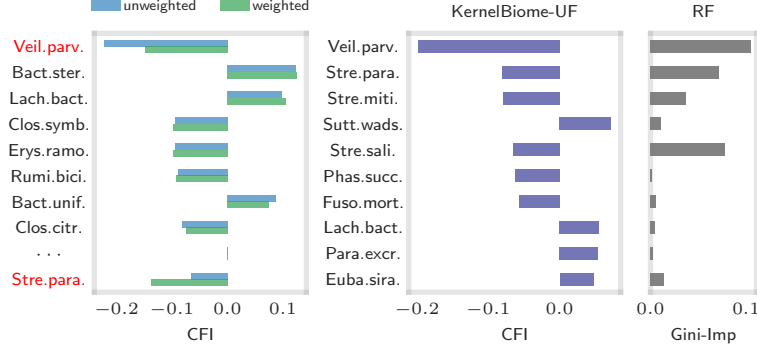


Figure 4: Left: Comparison of CFI based on *KernelBiome* unweighted (top, blue) and *KernelBiome* weighted with W as in (7) (bottom, green). The weighting ensures, as expected, that *Veillonella parvula* and *Streptococcus parasanguinis* (highlighted) receive similar CFI values. Middle: CFI based on *KernelBiome-UF*. Compared to the unweighted CFIs on the left, the weighted CFIs have upweighted species from the *Streptococcus* genus Gini importance based on RF (Right).

One type of prior information that is generally available for microbiome datasets is the genetic relation encoded in the phylogenetic tree. Applying the proposed UniFrac-weighting (see Appendix B.3) to the Cirrhosis dataset, results in the CFIs given in Figure 4 (middle). Here, we only show the top 10 species with the largest absolute CFI, a plot showing all species is provided in Appendix C.3. The CFIs corresponding to *KernelBiome* (Fig. 4: left, blue) and *KernelBiome-UF* (Fig. 4: middle) are different. In particular, in the weighted case, three species from the *Streptococcus* genus are part of the top 8 species with largest absolute CFI, while non of them appear in the unweighted case. As species from the same genus are close in terms of UniFrac-distance the weighted model will favor these species if all of them have similar effects on the response.

Finally, we have also provided the commonly employed Gini importance based on a fitted random forest in Figure 4 (right). There are significant differences between the Gini importance and both the weighted and unweighted CFIs.

3.3 Model analysis with *KernelBiome*

Lastly, we highlight potential further ways to analyze the model based on the Cirrhosis dataset. Using the best fitting kernel, in this case an Aitchison kernel with $c = 10^{-5}$, we conduct a kernel-based dimensionality reduction to visualize relative abundance data (see Appendix E.2).

The resulting plot is shown in Figure 5 (left). It can be used to detect patterns in the

data and investigate outliers, giving further insights into the fitted model. Furthermore, as discussed in Section 2.3.2 the fitted kernel also provides a data-driven diversity, in Figure 5 (right) we compare it with the commonly employed Gini-Simpson diversity (which itself corresponds to the linear kernel diversity).

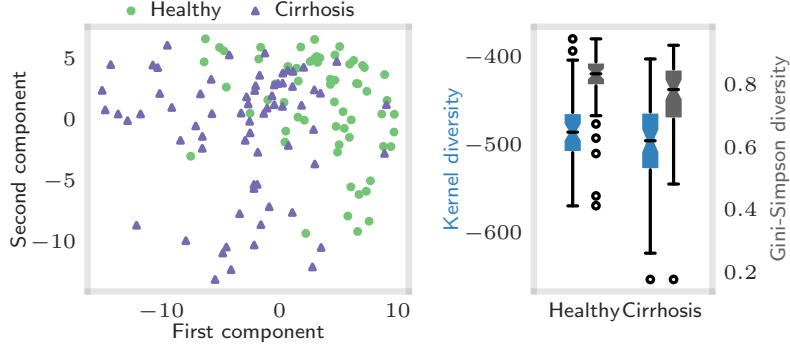


Figure 5: Left: MDS plot using the top-fitted kernel, Aitchison kernel with $c = 10^{-5}$. Right: Kernel diversity based on the same kernel.

4 Discussion and conclusions

In this work, we propose the **KernelBiome** framework for supervised learning with compositional covariates consisting of two main ingredients: data-driven model selection and model interpretation. Our approach is based on a flexible family of kernels targeting the structure of microbiome data, and is able to work with different kernel-based algorithms such as SVM and kernel ridge regression. It is also possible to incorporate prior knowledge, which is crucial in microbiome data analysis. We compare **KernelBiome** with other state-of-the-art approaches on two real datasets for classification and regression tasks, and show that **KernelBiome** achieves improved or comparable results. Moreover, **KernelBiome** provides multiple ways to extract interpretable information from the fitted model. Two novel measures, CFI and CPD, can be used to analyze how each component affects the response. We prove the consistency of these two measures and also demonstrate them via simulated and real datasets. **KernelBiome** also leverages the connection between kernels and distances to conduct distance-based analysis in a lower-dimensional space.

The **KernelBiome** package is provided as an open-source Python package that is ready to be installed via `pip`. An example of the entire workflow using **KernelBiome** is provided in the Github repository at <https://github.com/shimenghuang/KernelBiome>.

Appendix

The appendix is divided into the following sections.

A Details on CFI and CPD.

Formal definitions of perturbations and estimators related to CFI and CPD.

B Details on kernels included in `KernelBiome`

Overview of different kernel types, details on how they connect to distances and description of weighted kernels.

C Details and additional results for experiments in Section 3

Datasets pre-processing, parameter setup, construction of the weighting matrices with UniFrac-distance and further experiment results based on the Cirrhosis and Central-ParkSoil datasets.

D Additional experiments with simulated data

Consistency of CFI and CPD and comparison of CFI and CPD with their non-simplex counterparts.

E Background on kernels

Mathematical background on kernels and details on dimensionality and visualization with kernels.

F Proofs

G List of kernels implemented in `KernelBiome`

A Details on CFI and CPD

A.1 Perturbations

Formally, the multiplicative perturbation ψ and the fixed coordinate perturbation ϕ are defined as follows.

- For any $j \in \{1, \dots, p\}$, $x \in \mathbb{S}^{p-1}$ and $c \in [0, 1]$, define

$$\psi_j(x, c) := s_c(x^1, \dots, x^{j-1}, cx^j, x^{j+1}, \dots, x^p) \in \mathbb{S}^{p-1},$$

where $s_c = 1/(\sum_{\ell \neq j}^p x^\ell + cx^j)$.

- For any $j \in \{1, \dots, p\}$, $x \in \mathbb{S}^{p-1}$ with $\sum_{\ell \neq j}^p x^\ell > 0$ and $c \in [0, 1]$, define the intervened composition by

$$\phi_j(x, c) := (sx^1, \dots, sx^{j-1}, c, sx^{j+1}, \dots, sx^p) \in \mathbb{S}^{p-1},$$

where $s = (1 - c)/(\sum_{\ell \neq j}^p x^\ell)$.

A.2 Estimators

We propose to estimate CFI and CPD with the following two estimators.

- For i.i.d. observations X_1, \dots, X_n and a differentiable function $f : \mathbb{S}^{p-1} \rightarrow \mathbb{R}$, we estimate the CFI for all $j \in \{1, \dots, p\}$ as

$$\hat{I}_f^j = \frac{1}{n} \sum_{i=1}^n \left. \frac{d}{dc} f(\psi(X_i, c)) \right|_{c=1}.$$

- For i.i.d. observations X_1, \dots, X_n and a function $f : \mathbb{S}^{p-1} \rightarrow \mathbb{R}$, we estimate the CPD for all $j \in \{1, \dots, p\}$ and $z \in [0, 1]$ as

$$\hat{S}_f^j(z) = \frac{1}{n} \sum_{i=1}^n f(\phi(X_i, z)) - \frac{1}{n} \sum_{i=1}^n f(X_i).$$

B Details on kernels included in KernelBiome

B.1 Overview of kernels

In this section, we give additional details on the kernels used in **KernelBiome**. A full list of all kernels and their corresponding metrics together with a visualization on \mathbb{S}^2 is given in Appendix G.

As discussed in the main paper, we consider four types of kernels.

- **Euclidean** These are kernels that are used on Euclidean space but restricted to the simplex. This includes the *linear kernel* and the *RBF kernel*.
- **Probability distribution** These are kernels that are constructed from metrics between probability distributions. **KernelBiome** includes two parametric classes of kernels, the *Hilbertian kernel* and the *generalized-JS kernel*. These kernels correspond to multiple well-known metrics on probabilities such as the *chi-squared metric*, the *total-variation metric*, the *Hellinger metric* and the *Jensen-Shannon metric*.
- **Aitchison geometry** These are kernels that are constructed by using the centered log-ratio transform to project data on the simplex into Euclidean space and then combining it with a Euclidean kernel. **KernelBiome** includes the *Aitchison kernel* and the *Aitchison RBF kernel*. In order to allow for zeros, we shift each point by a constant $c > 0$ before applying the centered log-ratio transform.

- **Riemannian manifold** These kernels are connected to the simplex via multinomial distributions and have been shown to empirically perform well on sparse text data that is mapped into the simplex. `KernelBiome` contains the *heat-diffusion kernels*.

For each type of kernel there are multiple parameter setting. The default settings for `KernelBiome` consider all kernels given by the parameter combinations in Table B1.

Geometry	Kernel	Parameters	# of valid kernels
Euclidean	linear	none	1
	RBF	$\sigma \in \{\sqrt{m_1}, 0.5m_1, m_1, m_1^{1.5}, m_1^2, m_1^{2.5}, 10m_1, 100m_1\}$	8
Probability distributions	generalized-JS	$a \in \{1, 10, \infty\}, b \in \{0.5, 1, 10, \infty\}$	9
	Hilbertian	$a \in \{1, 10, \infty\}, b \in \{-1, -10, -\infty\}$	8
Aitchison geometry	Aitchison	$c \in \{10^{-7}, 10^{-6}, 10^{-5}, 10^{-4}, 10^{-3}\}$	5
	Aitchison-RBF	$c \in \{10^{-7}, 10^{-6}, 10^{-5}, 10^{-4}, 10^{-3}\},$	40
		$\sigma \in \{\sqrt{m_2}, 0.5m_2, m_2, m_2^{1.5}, m_2^2, m_2^{2.5}, 10m_2, 100m_2\}$	
Riemannian manifold	heat-diffusion	$t \in \{0.9, 0.95, 1., 1.05, 1.1\} \times \frac{1}{4\pi}$	5

Table B1: Default parameter grid in `KernelBiome`. m_1 and m_2 are the median value of the squared Euclidean distance of the original and the log clr-transformed data respectively. For kernels with multiple parameters all valid combinations are considered. In total this results in 76 kernels.

B.1.1 Connecting positive definite kernels to metrics

All kernels included in `KernelBiome` are positive definite. By Theorem E.2 it can be shown that each kernel k defines a unique metric d_k on the simplex via

$$d_k(x, y) = \sqrt{k(x, x) + k(y, y) - 2k(x, y)}. \quad (8)$$

Furthermore, each kernel k also induces a unique RKHS \mathcal{H}_k with reproducing kernel k . It can be shown that the distance between two points on the simplex $x, y \in \mathbb{S}^{p-1}$ measured by d_k corresponds to the distance between the embedded features in \mathcal{H}_k , that is,

$$\|k(x, \cdot) - k(y, \cdot)\|_{\mathcal{H}_k} = d_k(x, y).$$

The feature embedding $x \mapsto k(x, \cdot)$ induced by a kernel therefore preserves the distances d_k . A useful aspect of kernel methods, is that they allow a post-analysis based on the embedded features, see also Appendix E.2.

Kernels can be shifted in such a way that the origin in the induced RKHS changes but the metric in (8) remains fixed (see Lemma E.1). A natural origin in the simplex is given

by the point $u = (\frac{1}{p}, \dots, \frac{1}{p})$, therefore we have shifted all kernels such that $k(u, \cdot) \equiv 0$ and hence correspond to the origin in \mathcal{H}_k . In Appendix E.1, we provide a short overview of the mathematical results that connect kernels and metrics.

B.2 Weighted kernels - including prior information

In this section, we discuss how to include prior knowledge, e.g. phylogenetic information, into the simplex kernels. We assume the information is encoded in a matrix $W \in \mathbb{R}^{p \times p}$ where each element corresponds to a measure of similarity between components. That is, $W_{i,j}$ is large if components i and j are similar (or related) and small otherwise. We assume that W is symmetric, positive semi-definite and all entries in W are non-negative.

The linear kernel and all kernels based on probability distributions have the form given in (5) and we therefore define the weighted version by

$$k_W(x, y) = \sum_{j,\ell=1}^p W_{j,\ell} \cdot k_0(x^j, y^\ell). \quad (9)$$

The weighted versions of the remaining kernels are defined individually. A full list of the weighted kernels is given in Appendix G.1.

B.2.1 Validity of weighted kernels

In order to use the proposed weighted kernels, we need to ensure that they are indeed positive definite. In the following, we prove this for the weighted versions of the *linear kernel*, the *Hilbertian kernel*, the *Generalized-JS kernel*, the *RBF kernel* and the *Aitchison kernel*. We do not prove it for the *Aitchison RBF kernel* and the *Heat Diffusion kernel* and only note that they appear to be positive definite from our empirical evaluations.

We begin by showing that the kernel defined in (9) is positive definite whenever $k_0 : [0, 1] \times [0, 1] \rightarrow \mathbb{R}$ is positive definite. To see this, fix $x_1, \dots, x_n \in \mathbb{S}^{p-1}$ and $\alpha \in \mathbb{R}^n$ and denote by $K_W \in \mathbb{R}^{n \times n}$ the kernel Gram-matrix based on x_1, \dots, x_n and kernel k_W . Then,

$$\begin{aligned} \alpha^\top K_W \alpha &= \sum_{i,r=1}^n \sum_{j,\ell=1}^p \alpha_i \alpha_r W_{j,\ell} k_0(x_i^j, x_r^\ell) \\ &= \sum_{j,\ell=1}^p W_{j,\ell} \left(\sum_{i,r=1}^n \alpha_i \alpha_r k_0(x_i^j, x_r^\ell) \right). \end{aligned}$$

Since k_0 is positive definite, it holds that $\sum_{i,r} \alpha_i \alpha_r k_0(x_i^j, x_r^\ell) \geq 0$ and hence $\alpha^\top K_W \alpha \geq 0$ since all entries in W are non-negative.

We now go over the individual weighted kernels and argue that they are positive definite.

- **Linear kernel**

Since \mathbb{R} is a Hilbert space with the inner product xy which induces the $|x - y|$ it follows that the squared distance $d_{\text{Linear}}^2(x, y) := (x - y)^2$ is Hilbertian as well. Applying Theorem E.1 we know that the distance is of negative type. Thus, based on the one-dimensional squared linear distance d_{Linear}^2 , we apply Theorem E.2 with $x_0 = \frac{1}{p}$ to construct the following positive definite kernel k_0 defined for all $x, y \in [0, 1]$ by

$$k_0(x, y) := -\frac{1}{2}(x - y)^2 + \frac{1}{2}(x - \frac{1}{p})^2 + \frac{1}{2}(\frac{1}{p} - y)^2 = xy - \frac{x}{p} - \frac{y}{p} + \frac{1}{p^2}.$$

Comparing this with our weighted linear kernel in Appendix G.1, we see that the weighted linear kernel has the form (9) and is therefore positive definite by the above argument.

- **Hilbertian kernel** As shown by Hein and Bousquet (2005) the distance $d_{\text{Hilbert}} : \mathbb{R}_+ \times \mathbb{R}_+ \rightarrow \mathbb{R}$ defined for all $x, y \in \mathbb{R}_+$ by

$$d_{\text{Hilbert}}^2(x, y) = \frac{2^{\frac{1}{b}} \left[x^a + y^a \right]^{\frac{1}{a}} - 2^{\frac{1}{a}} \left[x^b + y^b \right]^{\frac{1}{b}}}{2^{\frac{1}{a}} - 2^{\frac{1}{b}}}$$

is a Hilbertian metric on \mathbb{R}_+ . Applying Theorem E.2 with $x_0 = \frac{1}{p}$ results in a positive definite kernel k_0 that when combined as in (9) results in the proposed weighted Hilbertian kernels in Appendix G.1. Therefore, we have shown that the weighted Hilbertian kernels are positive definite as long as W has non-negative entries.

- **Generalized-JS kernel** Similarly the weighted Generalized-JS kernels in Appendix G.1 can all be decomposed as in (9) with a one-dimensional kernels k_0 on $[0, 1]$. Topsøe (2003) show that all these k_0 can be generated using Theorem E.2 with $x_0 = \frac{1}{p}$ based on Hilbertian metrics. Hence, all weighted Generalized-JS kernels are positive definite as long as W has non-negative entries.
- **Aitchison kernel** To show that the weighted Aitchison kernel (defined in Appendix G.1) is positive definite, we first define the mapping $\Phi : \mathbb{S}^{p-1} \rightarrow \mathbb{R}^p$ by $\Phi(x) := \frac{x+c}{g(x+c)}$. Then, the weighted Aitchison kernel is given by

$$k(x, y) = \Phi(x)^\top W \Phi(y).$$

Since W is symmetric and positive semi-definite there exists $M \in \mathbb{R}^{p \times p}$ such that $W = M^\top M$. Therefore, for any $\alpha \in \mathbb{R}^n$ and $x_1, \dots, x_n \in \mathbb{S}^{p-1}$ it holds that

$$\sum_{i,r} \alpha_i \alpha_r k(x_i, x_r) = \sum_{i,r} \alpha_i \alpha_r (M \Phi(x_i))^\top M \Phi(x_r) \geq 0.$$

Hence, k is positive definite.

- **RBF kernel** Using the symmetry of W the weighted RBF kernel can be expressed as follows

$$\begin{aligned}
k(x, y) &= \exp \left(-\frac{1}{\sigma^2} \sum_{j,\ell=1}^p W_{j,\ell} (x^j - y^\ell)^2 \right) \\
&= \underbrace{\exp \left(-\frac{1}{\sigma^2} \sum_{j,\ell=1}^p W_{j,\ell} (x^j)^2 \right) \exp \left(-\frac{1}{\sigma^2} \sum_{j,\ell=1}^p W_{j,\ell} (y^\ell)^2 \right)}_{=:A(x,y)} \underbrace{\exp \left(\frac{2}{\sigma^2} \sum_{j,\ell=1}^p W_{j,\ell} x^j y^\ell \right)}_{=:B(x,y)}
\end{aligned}$$

The function A is a positive definite kernel since it is the inner-product of a feature mapping. The function B can be shown to be a kernel by considering the Taylor expansion of the exponential function and using that sums and limits of positive definite kernels are again positive definite together with the fact that W is positive semi-definite. Therefore, the weighted RBF kernel is positive definite.

B.3 UniFrac-Weighting

In this section, we show how prior information based on the UniFrac-Distance (Lozupone and Knight, 2005) can be encoded into a weight matrix $W \in \mathbb{R}^{p \times p}$. Depending on the application at hand different distances can be used in a similar way. The UniFrac-Distance is a β -diversity measure that uses phylogenetic information to compare two compositional samples $x, y \in \mathbb{S}^{p-1}$. Each element of the sample is hereby placed on a phylogenetic tree. The distance between both samples is computed via quantification of overlapping branch length, that is,

$$\text{UniFrac-Distance}(x, y) = \frac{\text{sum of unshared branch length of } x \text{ and } y}{\text{sum of all tree branch length of } x \text{ and } y} \in [0, 1].$$

Based on the UniFrac-Distance, we define two similarity matrices $M^A, M^B \in [0, 1]^{p \times p}$ for all $i, j \in \{1, \dots, p\}$ by

$$\begin{aligned}
M_{i,j}^A &:= 1 - \text{UniFrac-Distance}(e_i, e_j), \\
M_{i,j}^B &:= \sum_{\ell=1}^p \text{UniFrac-Distance}(e_i, e_\ell) \cdot \text{UniFrac-Distance}(e_j, e_\ell),
\end{aligned}$$

where $e_i, e_j \in \mathbb{S}^{p-1}$ with 1 on the i -th and j -th coordinate, respectively. M^A and M^B are two options of encoding the UniFrac-Distance as a similarity. M^B is positive semi-definite by construction, while this is not true for M^A and should be checked empirically. We recommend using M^A whenever it is positive semi-definite.

We then construct the weight matrix $W^{\text{UniFrac}} \in \mathbb{R}^{p \times p}$ by scaling M^* such that the rows

sum to one, that is,

$$W^{\text{UniFrac}} := DM^*D,$$

where $D = \text{diag}(\sigma_1, \dots, \sigma_p)$ and $\sigma_i = (\sum_{\ell=1}^p M_{i,\ell}^*)^{\frac{1}{2}}$. By construction, this weight matrix takes values in $[0, 1]$, is symmetric, has rows summing to one and is positive semi-definite if M^* is positive semi-definite.

C Details and additional results for experiments in Section 3

C.1 Preprocessing of microbiome datasets

The Cirrhosis dataset is obtained from the MLRepo github <https://github.com/knights-lab/MLRepo/tree/master/datasets/qin2014>, and the CentralParkSoil is obtained from <https://github.com/jacobbien/trac-reproducible/tree/main/CentralParkSoil/original>. We preprocess the two datasets by first aggregating the taxa to species level, then keeping only the high prevalence and high average relative abundance species. Prevalence of a species is the proportion of samples for which this species exists, and average relative abundance of a species is the average of relative abundance (counts of the species divided by total counts of species of each sample) across samples. Specifically, we keep species j that satisfy

$$\text{prevalence}_j \geq (\beta_0 + \text{average relative abundance}_j * \beta_1),$$

where β_0 and β_1 are fixed constants depending on the dataset. For the Cirrhosis dataset we chose $\beta_0 = 1$ and $\beta_1 = -10$ which results in 108 species. For the CentralParkSoil dataset, we chose $\beta_0 = 1.03$ and $\beta_1 = -100$ which results in 114 species. These constants were selected manually and chosen to reduce the number of species approximately 100.

C.2 Weighting matrix for weighted KernelBiome

The weight matrix W^{UniFrac} for the Cirrhosis dataset (Qin et al., 2014) and the CentralParkSoil dataset (Ramirez et al., 2014) are presented as heatmaps in Figure C1. Using our proposed weighted kernels (see Appendix G.1) with the UniFrac-based weight matrix W^{UniFrac} is different from incorporating the UniFrac-distance via kernel convolution as proposed by Zhao et al. (2015).

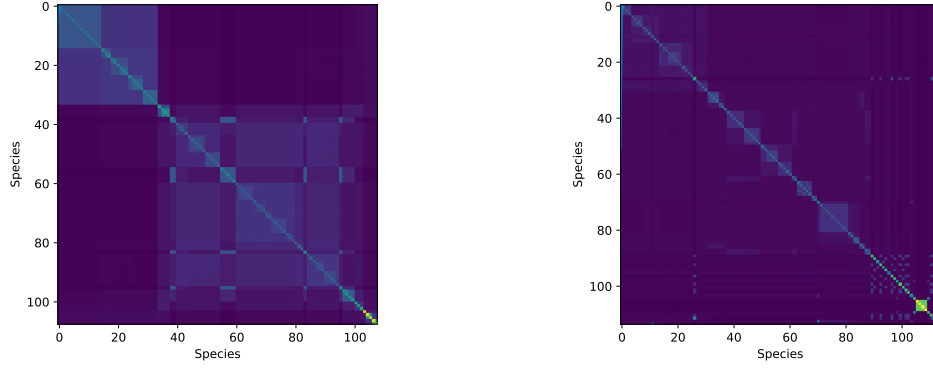


Figure C1: Visualization of the UniFrac weight $W^{\text{UniFrac}} = DM^A D$ for the pre-screened species (see Appendix C.1). Left: Cirrhosis dataset. Right: CentralParkSoil dataset.

C.3 CFI and CPD plots for Cirrhosis and CentralParkSoil datasets

The full list of CFI based on `KernelBiome` and `KernelBiome-UF`, as well as the Gini importance based on RF are given in Figure C4 and Figure C5 for the Cirrhosis and CentralParkSoil datasets respectively. For CPD, we include the top 10 species along with their corresponding CFI values based both unweighted `KernelBiome` and `KernelBiome-UF` estimator for the two datasets in Figure C2 and Figure C3.

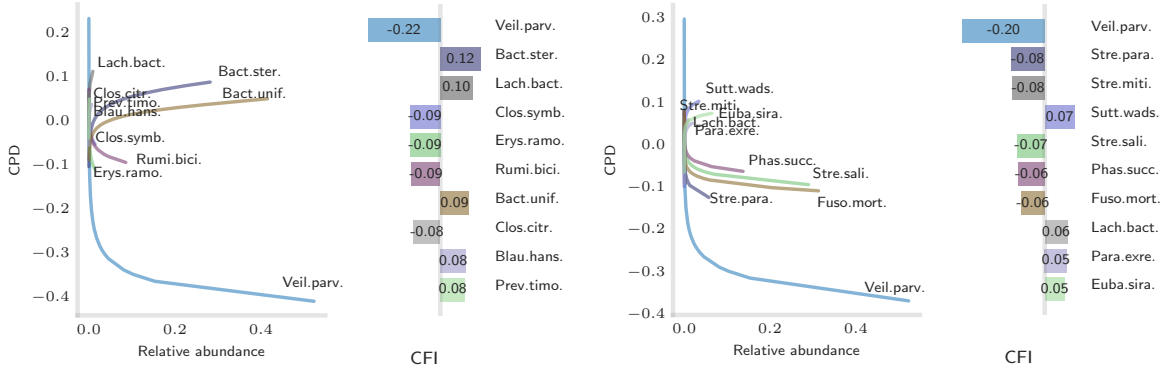


Figure C2: CPD and CFI of 10 species with the highest absolute CFI values for the Cirrhosis dataset based on unweighted `KernelBiome` estimator (left, best kernel: Aitchison with $c = 10^{-5}$) and `KernelBiome-UF` estimator (right: Aitchison with $c = 10^{-7}$).

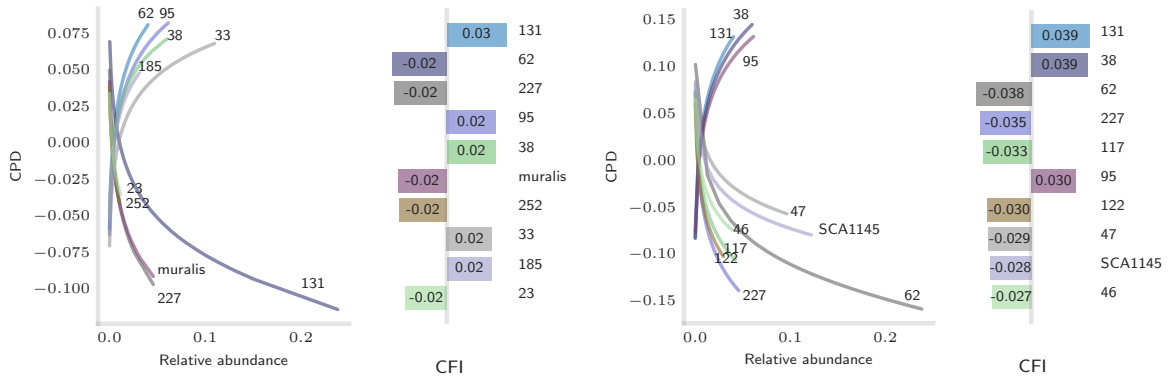


Figure C3: CPD and CFI of 10 species with the highest absolute CFI values for the Central-ParkSoil dataset based on unweighted **KernelBiome** estimator (left, best kernel: Aitchison-RBF with $c = 0.001$ and $g = 0.0023$) and **KernelBiome-UF** estimator (right, best kernel: Aitchison-RBF with $c = 0.001$ and $g = 0.0012$).



Figure C4: CFI based on KernelBiome, KernelBiome-UF, and Gini-importance based on RF for the Cirrhosis dataset.

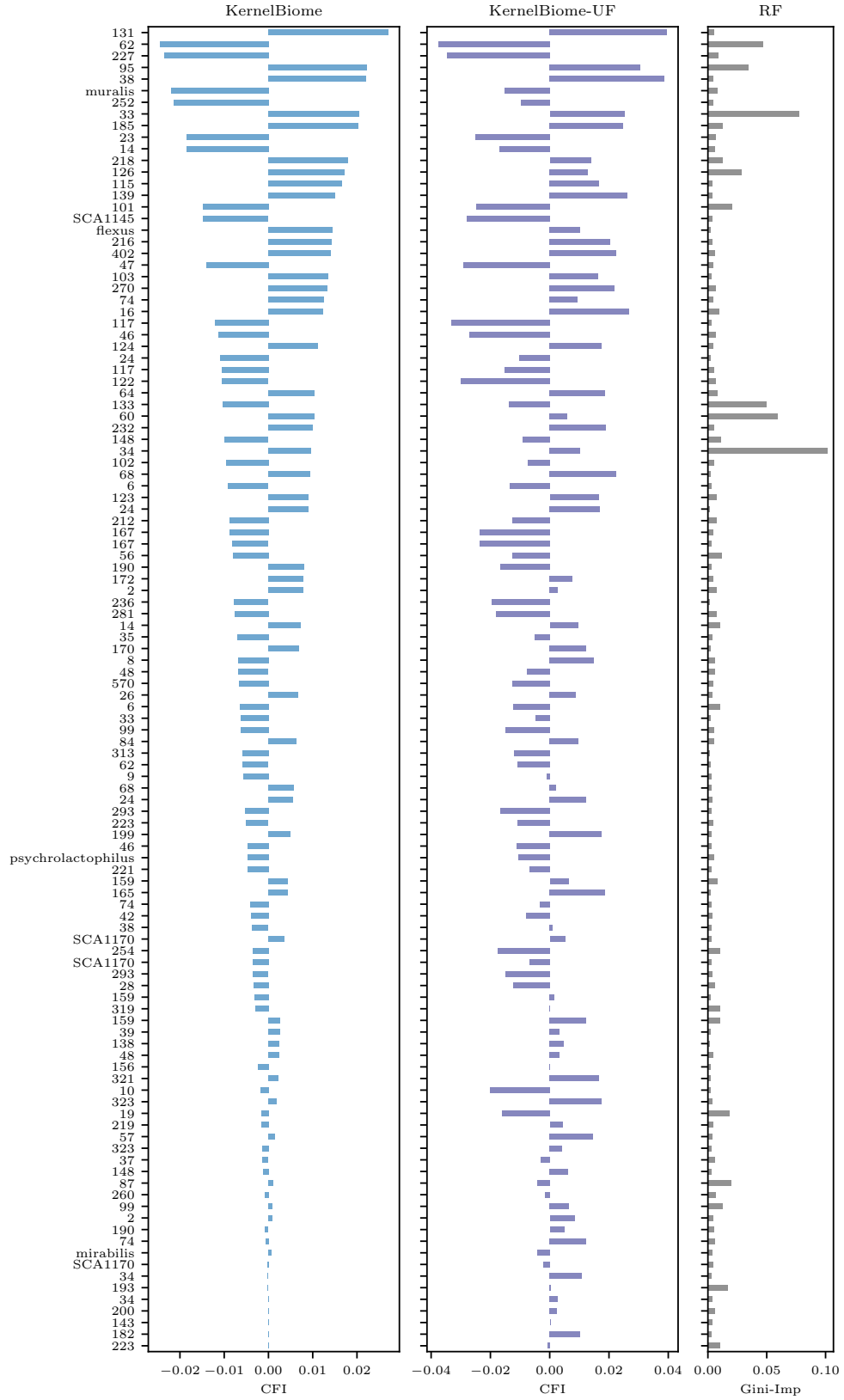


Figure C5: CFI based on KernelBiome, KernelBiome-UF, and Gini-importance based on RF for the CentralParkSoil dataset. Only some of the species labels are available in the dataset and the rest are labeled by a unique number.

D Additional experiments with simulated data

D.1 Consistency of CPD and CFI

We illustrate the consistency of CPD and CFI from Theorem 2.1 based on `KernelBiome` with the following example. Let k_{tv} be the total variation kernel and consider the function

$$f : x \mapsto 100 \cdot k_{\text{tv}}(z, x)$$

where

$$z = (0.06544714, 0.08760064, 0.17203408, 0.07502236, \\ 0.1642615, 0.03761901, 0.18255478, 0.13099514, 0.08446536) \in \mathbb{S}^8$$

is a fixed and randomly selected point.

Furthermore, we generate an i.i.d. dataset $(X_1, Y_1), \dots, (X_n, Y_n)$ based on the following 2 step generative model.

Step 1: Generate a random variable $\tilde{X} = (\tilde{X}^1, \dots, \tilde{X}^9)$ such that the three blocks $(\tilde{X}^1, \tilde{X}^2, \tilde{X}^3)$, $(\tilde{X}^4, \tilde{X}^5, \tilde{X}^6)$, and $(\tilde{X}^7, \tilde{X}^8, \tilde{X}^9)$ are i.i.d. from $\text{LogNormal}(0, \Sigma)$, where

$$\Sigma = \begin{pmatrix} 1 & 0.25 & -0.25 \\ 0.25 & 1 & 0.25 \\ -0.25 & 0.25 & 1 \end{pmatrix}$$

. Then, X_i is constructed by normalizing \tilde{X} , that is, $X_i = \tilde{X} / \sum_{j=1}^9 \tilde{X}^j$. The block structure adds non-trivial correlation structure between the compositional components.

Step 2: Generate Y_i based on X_i by

$$Y_i = f(X_i) + \epsilon_i$$

with $\epsilon_i \stackrel{iid}{\sim} \mathcal{N}(0, 1)$.

Based on one such dataset, we then estimate the CFI and CPD for a fitted `KernelBiome` estimator (using kernel ridge regression and default settings), and compare the estimates against the population CFI and CPD calculated from the true function f . In Figure D1, we report the mean squared deviations (MSD) for both CFI and CPD based on 100 such datasets for each sample size. As the sample size n increases the CFI and CPD estimates based on `KernelBiome` converge to the true population quantities.

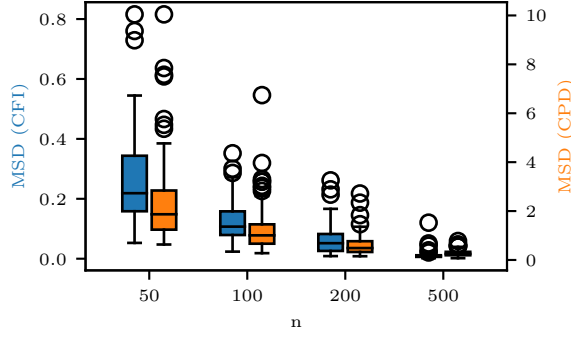


Figure D1: MSD of estimated CFI and CPD using `KernelBiome` estimator based on 100 random datasets for each sample size. For CPD, we calculate the true and estimated CPD based on 100 evenly spaced grid points within the range of $[0, 1]$ and the reported MSD is the average MSD over the 9 components. As the sample size n increases the CFI and CPD estimates based on `KernelBiome` converge to the true population quantities.

D.2 Comparing CFI and CPD with permutation importance and partial dependence plots

A common approach to assess the individual importance of features is permutation importance (PI). PI of the j -th feature is defined as the mean difference between the baseline mean squared error of a fitted model and the average mean squared error after permuting the j -th feature column a certain number of times. Partial dependence plots (PDPs) are a method describing how individual features contribute to a fitted model. For the j -th feature it describes its contribution by the function $z \mapsto \mathbb{E}[\hat{f}(X) \mid \text{do}(X^j = z)]$, where \hat{f} is the fitted model. Both PI and PDP can be misleading when used with compositional covariates. In this section, we illustrate this based on two examples. In both cases, the proposed adjusted measures CFI and CPD remain correct, while the PI and PDP are incorrect.

Consider the two functions

$$\begin{aligned} f_1 &: x \mapsto 10x^1 + 10x^2 \\ f_2 &: x \mapsto \frac{1 - x^2 - x^3}{1 - x^3}. \end{aligned} \tag{10}$$

For f_1 , changes in all coordinates affect the function value due to the simplex constraint. For f_2 , only changes in x^1 and x^2 affect the function value but not changes in x^3 . This is because on the simplex $f_2(x) = \frac{x^1}{x^1 + x^2}$. An importance measure should therefore associate a non-zero value to x^3 for f^1 and zero to x^3 for f^2 .

We now generate 200 i.i.d. observations X_1, \dots, X_{100} with $X_i \stackrel{d}{=} \tilde{X}_i / \sum_{j=1}^3 \tilde{X}_i^j$ for $\tilde{X}_i \stackrel{\text{i.i.d.}}{\sim} \text{LogNormal}(0, \text{Id}_3)^4$ and compute PI, PDP, CFI and CPD for each of the two functions. The

⁴ $\text{LogNormal}(\mu, \Sigma)$ denotes the log-normal distribution with location parameter μ and scale parameter Σ . Id_3 denotes the 3-dimensional identity matrix.

	f_1			f_2		
	x^1	x^2	x^3	x^1	x^2	x^3
CFI	0.85	0.87	-1.72	1.94	-1.94	0.00
FI	3.76	2.99	0.00	0.00	-4.72	-4.40
PI	11.35	5.87	0.00	0.00	34.90	25.39

Table D1: CFI, FI and PI for the two functions f_1 and f_2 defined in (10). Only CFI correctly attributes the effect of x^3 (marked in bold).

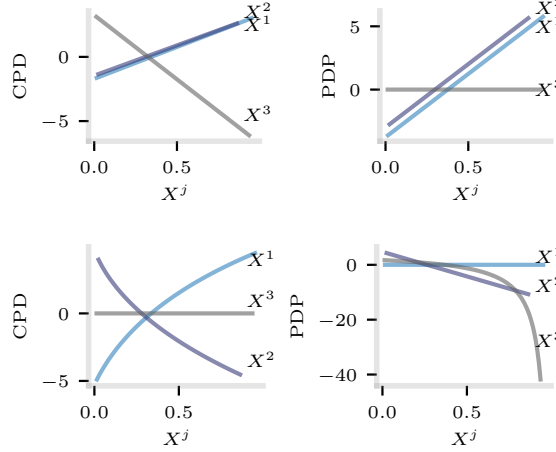


Figure D2: Top row: CPD and PDP plot based on f_1 . Bottom row: CPD and PDP plot based on f_2 . CPD reflects the true feature importance on the simplex while PDP does not.

results are given in Table D1 and Figure D2.

As expected, the CFI and also CPD correctly capture the behavior of the two functions. However, PI and PDP are incorrect in both cases: For f_1 the variable x^3 shows no effect both with PI and PDP and for f_2 the variable x^3 is falsely assigned a strong negative effect even though it does not affect the function value at all. In Table D1, we have additionally computed the standard feature influence (FI) given by $\mathbb{E}[\frac{d}{dx^j} \hat{f}(X)]$ due to Friedman (2001). It has the same problems as PI as it does not take into account the simplex structure.

E Background on kernels

E.1 Connection between metrics and kernels

Definition E.1 (Metric, semi-metric, and quasi-metric). A function $d : \mathcal{X} \times \mathcal{X} \rightarrow \mathbb{R}$ is called a *metric* if it satisfies

- (a) $d(x, x) = 0$,
- (b) $d(x, y) = d(y, x) \geq 0$,

$$(c) \quad d(x, y) \leq d(x, z) + d(y, z),$$

$$(d) \quad d(x, y) = 0 \Rightarrow x = y.$$

It is called a *semi-metric* if it satisfies (a)-(c), and a *quasi-metric* if it satisfies (a)-(b).

Definition E.2 (Function of negative type and Hilbertian metric). A quasi-metric $d : \mathcal{X} \times \mathcal{X} \rightarrow \mathbb{R}$ is called of *negative-type* if for all $n \in \mathbb{N}$, all $x_1, \dots, x_n \in \mathcal{X}$, and all $c_1, \dots, c_n \in \mathbb{R}$ with $\sum_{i=1}^n c_i = 0$, it holds that

$$\sum_{i,j=1}^n c_i c_j d^2(x_i, x_j) \leq 0. \quad (11)$$

If d is a (semi-)metric, then d is also called *Hilbertian*.

Theorem E.1 (Sufficient and necessary conditions for isometric embeddings). A quasi-metric space (X, d) can be isometrically embedded in a Hilbert space if and only if d is of negative type.

Proof. See Wells and Williams (2012, Theorem 2.4). □

Definition E.3 ((conditionally) positive definite kernels). A symmetric function $k : \mathcal{X} \times \mathcal{X} \rightarrow \mathbb{R}$ (i.e., $\forall x, y \in \mathcal{X}, k(x, y) = k(y, x)$) is called a *positive definite kernel* if and only if for all $n \in \mathbb{N}$, all $x_1, \dots, x_n \in \mathcal{X}$, and all $c_1, \dots, c_n \in \mathbb{R}$, it holds that

$$\sum_{i,j=1}^n c_i c_j k(x_i, x_j) \geq 0 \quad (12)$$

It is called a *conditional positive definite kernel* if instead of for all $c_1, \dots, c_n \in \mathbb{R}$ condition (12) only holds for all $c_1, \dots, c_n \in \mathbb{R}$ with $\sum_{i=1}^n c_i = 0$.

Lemma E.1. Let \mathcal{X} be a non-empty set, fix $x_0 \in \mathcal{X}$ and let $k, \tilde{k} : \mathcal{X} \times \mathcal{X} \rightarrow \mathbb{R}$ be symmetric functions satisfying for all $x, y \in \mathcal{X}$ that

$$k(x, y) = \tilde{k}(x, y) - \tilde{k}(x, x_0) - \tilde{k}(y, x_0) + \tilde{k}(x_0, x_0) \quad (13)$$

Then k is positive definite if and only if \tilde{k} is conditionally positive definite.

Proof. Fix $n \in \mathbb{N}$, $c_1, \dots, c_n \in \mathbb{R}$, and $x_0, x_1, \dots, x_n \in \mathcal{X}$. Let $c_0 = -\sum_{i=1}^n c_i$, then we have

$$\begin{aligned}
\sum_{i,j=0}^n c_i c_j \tilde{k}(x_i, x_j) &= \sum_{i,j=1}^n c_i c_j \tilde{k}(x_i, x_j) + \sum_{i=1}^n c_i c_0 \tilde{k}(x_i, x_0) \\
&\quad + \sum_{j=1}^n c_0 c_j \tilde{k}(x_j, x_0) + c_0 c_0 \tilde{k}(x_0, x_0) \\
&= \sum_{i,j=1}^n c_i c_j \tilde{k}(x_i, x_j) - \sum_{i,j=1}^n c_i c_j \tilde{k}(x_i, x_0) \\
&\quad - \sum_{i,j=1}^n c_i c_j \tilde{k}(x_j, x_0) + \sum_{i,j=1}^n c_i c_j \tilde{k}(x_0, x_0) \\
&= \sum_{i,j=1}^n c_i c_j [\tilde{k}(x_i, x_j) - \tilde{k}(x_i, x_0) - \tilde{k}(x_j, x_0) + \tilde{k}(x_0, x_0)] \\
&= \sum_{i,j=1}^n c_i c_j k(x_i, x_j).
\end{aligned} \tag{14}$$

Now, if \tilde{k} is conditionally positive definite, then (14) implies that $\sum_{i,j=1}^n c_i c_j k(x_i, x_j) \geq 0$, so k is positive definite; if k is positive definite, (14) implies that $\sum_{i,j=0}^n c_i c_j \tilde{k}(x_i, x_j) \geq 0$ so \tilde{k} is conditionally positive definite. This completes the proof of Lemma E.1. \square

Lemma E.2 (Shifted conditionally positive definite). Let \mathcal{X} be a non-empty set and let $k : \mathcal{X} \times \mathcal{X} \rightarrow \mathbb{R}$ be a positive definite kernel, then

$$\tilde{k}(x, y) = k(x, y) + f(x) + f(y)$$

is a conditionally positive definite kernel for all $f : \mathcal{X} \rightarrow \mathbb{R}$.

Proof. The proof follows the exact same argument as the proof of Lemma E.1. \square

Theorem E.2 (Connection between Hilbertian semi-metrics and positive definite kernels). Let $k : \mathcal{X} \times \mathcal{X} \rightarrow \mathbb{R}$ and $d : \mathcal{X} \times \mathcal{X} \rightarrow [0, \infty)$ be functions. If k is a positive definite kernel and d satisfies $d^2(x, y) = k(x, x) + k(y, y) - 2k(x, y)$, then d is a Hilbertian semi-metric. On the other hand, for any $x_0 \in \mathcal{X}$, if d is a Hilbertian semi-metric and k satisfies $k(x, y) = -\frac{1}{2}d^2(x, y) + \frac{1}{2}d^2(x, x_0) + \frac{1}{2}d^2(x_0, y)$, then k is a pd kernel.

The result is due to Schoenberg (1938).

Proof. We start with the first part. Assume that k is a positive definite kernel and d satisfies $d^2(x, y) = k(x, x) + k(y, y) - 2k(x, y)$. Then, d is indeed a semi-metric by the following arguments:

$$(a) \quad d(x, x) = \sqrt{k(x, x) + k(x, x) - 2k(x, x)} = 0,$$

(b) $d(x, y) = d(y, x)$, and since k is positive definite, let $c_1 = 1$, $c_2 = -1$, $x_1 = x$, and $x_2 = y$,

$$\begin{aligned} 0 \leq \sum_{i,j=1}^n c_i c_j k(x_i, x_j) &= k(x_1, x_1) - k(x_1, x_2) - k(x_2, x_1) + k(x_2, x_2) \\ &= k(x, x) + k(y, y) - 2k(x, y) \\ &= d(x, y) \end{aligned}$$

(c) Since k is a positive definite kernel, there exists a feature map ϕ_k from \mathcal{X} to an RKHS \mathcal{H}_k , and we have

$$\begin{aligned} \|\phi_k(x) - \phi_k(y)\|_{\mathcal{H}_k}^2 &= \langle \phi_k(x) - \phi_k(y), \phi_k(x) - \phi_k(y) \rangle_{\mathcal{H}_k} \\ &= \langle \phi_k(x), \phi_k(x) \rangle_{\mathcal{H}_k} + \langle \phi_k(y), \phi_k(y) \rangle_{\mathcal{H}_k} - 2\langle \phi_k(x), \phi_k(y) \rangle_{\mathcal{H}_k} \\ &= k(x, x) + k(y, y) - 2k(x, y) \\ &= d^2(x, y) \end{aligned}$$

Therefore, $d(x, z) \leq d(x, y) + d(y, z)$ follows from the triangle inequality of a norm.

To show d is also Hilbertian, take any $n \in \mathbb{N}$, any $x_1, \dots, x_n \in \mathcal{X}$, and any $c_1, \dots, c_n \in \mathbb{R}$, we have

$$\begin{aligned} \sum_{i,j=1}^n c_i c_j d(x_i, x_j) &= \sum_{i=1}^n c_i k(x_i, x_i) \sum_{j=1}^n c_j + \sum_{j=1}^n c_j k(x_j, x_j) \sum_{i=1}^n c_i \\ &\quad - 2 \sum_{i,j=1}^n c_i c_j k(x_i, x_j) \\ &= -2 \sum_{i,j=1}^n c_i c_j k(x_i, x_j) \leq 0 \quad (\text{since } k \text{ is positive definite}). \end{aligned}$$

This proves the first part of the theorem.

For the second part, assume that d is a Hilbertian semi-metric and k satisfies $k(x, y) = -\frac{1}{2}d^2(x, y) + \frac{1}{2}d^2(x, x_0) + \frac{1}{2}d^2(x_0, y)$. Then, since d is Hilbertian, $-d^2$ satisfies the requirement of a conditionally positive definite kernel (with the additional property that $-d^2(x, x) = 0$). Hence, by Lemma E.1, k is indeed positive definite. This completes the proof of Theorem E.2. \square

E.2 Dimensionality reduction and visualization with kernels

One important benefit of using the kernel approach is that we can leverage the kernels for dimensionality reduction and visualization, so that one can identify outliers in the data and further investigate them. In this section, we provide a short introduction on how to use kernels

for multi-dimensional scaling and connect it to kernel PCA (Schölkopf et al., 2002).

Kernel methods project the compositional data into a (potentially) high-dimensional RKHS \mathcal{H}_k , which we now want to project into the low dimensional Euclidean space \mathbb{R}^l (with $l \ll p$) such that the lower dimensional representation preserves information that helps separate the observations of different traits in the RKHS. That is, given observations $x_1, \dots, x_n \in \mathbb{S}^p$ and a kernel k , we would like to define a map $\Phi : \mathcal{H}_k \rightarrow \mathbb{R}^l$ such that

$$\sum_{i,j=1}^n \|\langle k(x_i, \cdot), k(x_j, \cdot) \rangle_{\mathcal{H}_k} - \langle \Phi(k(x_i, \cdot)), \Phi(k(x_j, \cdot)) \rangle_{\mathbb{R}^l}\|^2$$

is minimized. In matrix notation, this corresponds to solving

$$\arg \min_{Z \in \mathbb{R}^{n \times l}} \|K - ZZ^T\|^2,$$

where the rows of Z are $z_i = \Phi(k(x_i, \cdot)) \in \mathbb{R}^l$ for all $i \in \{1 \dots, n\}$ and $K \in \mathbb{R}^{n \times n}$ is the kernel Gram-matrix.

This is similar to the classical multidimensional scaling (MDS) but measuring the similarity in the RKHS instead of in Euclidean space. By the Eckart-Young theorem (Eckart and Young, 1936), this minimization problem can be solved via the eigendecomposition of the matrix $K = V\Sigma V^T$, and the optimal solution is

$$Z_{\text{opt}} = (V_1, \dots, V_l)(\Sigma_{:l})^{\frac{1}{2}},$$

where V_1, \dots, V_l are the first l columns of V and $\Sigma_{:l}$ is the upper-left $(l \times l)$ -submatrix of Σ . The optimal projection Φ_{opt} is then given for all $f \in \mathcal{H}_k$ by

$$\Phi_{\text{opt}}(f) = (\Sigma_{:l})^{-\frac{1}{2}}(V_1, \dots, V_l)^T \begin{pmatrix} \langle f, k(x_1, \cdot) \rangle_{\mathcal{H}_k} \\ \vdots \\ \langle f, k(x_n, \cdot) \rangle_{\mathcal{H}_k} \end{pmatrix}. \quad (15)$$

This in particular allows to project a new observations $w \in \mathbb{S}^{p-1}$ with the same projection that is $w \mapsto \Phi_{\text{opt}}(k(w, \cdot))$.

The projection in (15) depends on the origin of the RKHS \mathcal{H}_k . To remove this dependence, it may therefore be desirable to consider a centered version of the optimal projection. This can be achieved by considering the RKHS $\tilde{\mathcal{H}}_k$ consisting of the functions $\tilde{f}(\cdot) = f(\cdot) - \frac{1}{n} \sum_{i=1}^n k(x_i, \cdot)$ with $f \in \mathcal{H}_k$. To compute the optimal centered projection (15) for the RKHS $\tilde{\mathcal{H}}_k$, we only need to perform double centering on the kernel matrix K , i.e., $\tilde{K} = HKH$, where $H = I - \frac{1}{n} \mathbf{1}\mathbf{1}^T$ and replace $k(x_\ell, \cdot)$ by $\tilde{k}(x_\ell, \cdot) = k(x_\ell, \cdot) - \frac{1}{n} \sum_{i=1}^n k(x_i, \cdot)$. With the centering step, this procedure is equivalent to kernel PCA (Schölkopf et al., 2002). The steps to obtain the lower-dimensional representation in matrix form are given in Algo-

rithm 1.

Algorithm 1 Dimensionality reduction with kernels

Input: Training data $X_1, \dots, X_n \in \mathbb{S}^{p-1}$, visualization data $X_1^{\text{new}}, \dots, X_m^{\text{new}} \in \mathbb{S}^{p-1}$ (can be same as training data), kernel function k , dimension $l \in \{1, \dots, p\}$, indicator whether to use centering $\text{CenterK} \in \{\text{True}, \text{False}\}$

Output: l -dimensional representation $Z = (Z_1, \dots, Z_m)^\top \in \mathbb{R}^{m \times l}$

```

1: # Define centering function
2: function CENTERKERNELMATRIX( $K, \tilde{K}$ )
3:    $K^{\text{center}} \leftarrow \tilde{K} - \frac{1}{n} \mathbf{1} \mathbf{1}^T K - \frac{1}{n} \tilde{K} \mathbf{1} \mathbf{1}^T + \frac{1}{n^2} \mathbf{1} \mathbf{1}^T K \mathbf{1} \mathbf{1}^T$ 
4:   return  $K^{\text{center}}$ 
5: end function

6: # Compute kernel matrix for training data
7: for  $i, j = 1, \dots, n$  do
8:    $K_{ij} \leftarrow k(X_i, X_j)$ 
9: end for

10: # Compute kernel matrix for visualization data
11: for  $i = 1, \dots, m$  and  $j = 1, \dots, n$  do
12:    $K_{ij}^{\text{new}} \leftarrow k(X_i^{\text{new}}, X_j)$ 
13: end for

14: # Center kernel matrices
15: if  $\text{CenterK}$  then
16:    $K^{\text{new}} \leftarrow \text{CenterKernelMatrix}(K, K^{\text{new}})$ 
17:    $K \leftarrow \text{CenterKernelMatrix}(K, K)$ 
18: end if

19: # Compute  $l$ -dimensional representation
20:  $V, \Sigma \leftarrow$  eigenvalue decomposition of  $K$ 
21:  $Z \leftarrow K^{\text{new}}(V_1, \dots, V_l)(\Sigma_{:l})^{-\frac{1}{2}}$ 

22: return  $Z$ 

```

F Proofs

F.1 Proof of Proposition 2.1

Proof. We start with the CFI. Fix $j \in \{1, \dots, p\}$ and $x \in \mathbb{S}^{p-1}$, then we can compute the derivative using the chain rule and the explicit form of the perturbation ψ as follows

$$\begin{aligned}
\frac{d}{dc}f(\psi_j(x, c)) &= \left\langle \nabla f(\psi_j(x, c)), \frac{d}{dc}\psi_j(x, c) \right\rangle \\
&= \left\langle \nabla f(\psi_j(x, c)), \frac{d}{dc}s_c(x^1, \dots, x^{j-1}, cx^j, x^{j+1}, \dots, x^p)^\top \right\rangle \\
&= \left\langle \nabla f(\psi_j(x, c)), \frac{d}{dc} \frac{1}{\sum_{\ell \neq j} x^\ell + cx^j} (x^1, \dots, x^{j-1}, cx^j, x^{j+1}, \dots, x^p)^\top \right\rangle \\
&= \left\langle \nabla f(\psi_j(x, c)), \frac{-x^j}{(\sum_{\ell \neq j} x^\ell + cx^j)^2} \right. \\
&\quad \left. (x^1, \dots, x^{j-1}, cx^j x^j - x^j (\sum_{\ell \neq j} x^\ell + cx^j), x^{j+1}, \dots, x^p)^\top \right\rangle.
\end{aligned}$$

Evaluating, the derivative at $c = 1$ leads to

$$\frac{d}{dc}f(\psi_j(x, c))|_{c=1} = \langle \nabla f(x), x^j(e_j - x) \rangle, \quad (16)$$

where we used that $\psi_j(x, 1) = x$. Moreover, the gradient of f in the case of the log-contrast model is given by

$$\nabla f(x) = \left(\frac{\beta_1}{x^1}, \dots, \frac{\beta_p}{x^p} \right)^\top. \quad (17)$$

Combining (16) and (17) together with the constraint $\sum_{k=1}^p \beta_k = 0$ implies that

$$\frac{d}{dc}f(\psi_j(x, c))|_{c=1} = -x^j \sum_{k \neq j} \beta_k + \beta^j(1 - x^j) = \beta_j.$$

Hence, taking the expectation leads to

$$I_j^j = \mathbb{E}[\frac{d}{dc}f(\psi_j(X, c))|_{c=1}] = \beta_j,$$

which proves the first part of the proposition.

Next, we show the result for the CPD. Fix $j \in \{1, \dots, p\}$ and $z \in [0, 1]$. Then $S_f^j(z)$ for

the log-contrast model can be computed as follows

$$\begin{aligned}
S_f^j(z) &= \mathbb{E}[f(\phi_j(X, z))] - \mathbb{E}[f(X)] \\
&= \sum_{\ell=1}^p \beta_\ell \mathbb{E}[\log(\phi_j(X, z)^\ell)] - \mathbb{E}[f(X)] \\
&= \sum_{\ell \neq j}^p \beta_\ell \mathbb{E}[\log(sX^\ell)] + \beta_j \log(z) - \mathbb{E}[f(X)] \\
&= \beta_j \log(z) + \sum_{\ell \neq j}^p \beta_\ell \mathbb{E}[\log(s)] + \sum_{\ell \neq j}^p \beta_\ell \mathbb{E}[\log(X^\ell)] - \mathbb{E}[f(X)],
\end{aligned}$$

where $s = (1 - z)/(\sum_{\ell \neq j}^p X^\ell)$. Using $\beta^j = -\sum_{\ell \neq j}^p \beta_\ell$ (which follows from the log-contrast model constraint on β) we can simplify this further and get

$$\begin{aligned}
S_f^j(z) &= \beta_j \log(z) + \sum_{\ell \neq j}^p \beta_\ell \mathbb{E}[\log(1 - z)] - \sum_{\ell \neq j}^p \beta_\ell \mathbb{E}[\log(\sum_{k \neq j}^p X^k)] + \sum_{\ell \neq j}^p \beta_\ell \mathbb{E}[\log(X^\ell)] - \mathbb{E}[f(X)] \\
&= \beta_j \log(z) - \beta_j \mathbb{E}[\log(1 - z)] + \beta_j \mathbb{E}[\log(\sum_{k \neq j}^p X^k)] + \sum_{\ell \neq j}^p \beta_\ell \mathbb{E}[\log(X^\ell)] - \mathbb{E}[f(X)] \\
&= \beta_j \log\left(\frac{z}{1 - z}\right) + \beta_j \mathbb{E}[\log(\sum_{k \neq j}^p X^k)] + \sum_{\ell \neq j}^p \beta_\ell \mathbb{E}[\log(X^\ell)] - \sum_{\ell=1}^p \beta_\ell \mathbb{E}[\log(X^\ell)] \\
&= \beta_j \log\left(\frac{z}{1 - z}\right) + c,
\end{aligned}$$

with $c = \beta_j \mathbb{E}[\log(\sum_{k \neq j}^p X^k)] + \sum_{\ell \neq j}^p \beta_\ell \mathbb{E}[\log(X^\ell)] - \sum_{\ell=1}^p \beta_\ell \mathbb{E}[\log(X^\ell)]$. Finally, assume $\beta^j = 0$, then it holds that

$$c = \sum_{\ell \neq j}^p \beta_\ell \mathbb{E}[\log(X^\ell)] - \sum_{\ell \neq j}^p \beta_\ell \mathbb{E}[\log(X^\ell)] = 0.$$

This completes the proof of Proposition 2.1. \square

F.2 Proof of Theorem 2.1

Proof. We first prove (i). To see this, we apply the triangle inequality to get that

$$|\hat{I}_{\hat{f}_n}^j - I_{f^*}^j| \leq \underbrace{|\hat{I}_{\hat{f}_n}^j - \hat{I}_{f^*}^j|}_{=: A_n} + \underbrace{|\hat{I}_{f^*}^j - I_{f^*}^j|}_{=: B_n}. \quad (18)$$

Next, we consider the two terms A_n and B_n separately. We begin with A_n , by using the definition of the CFI together with (16) from the proof of Proposition 2.1. This leads to

$$\begin{aligned}
A_n &= \left| \frac{1}{n} \sum_{i=1}^n \left(\frac{d}{dc} \hat{f}_n(\psi(X_i, c)|_{c=1}) - \frac{d}{dc} f^*(\psi(X_i, c)|_{c=1}) \right) \right| \\
&= \left| \frac{1}{n} \sum_{i=1}^n \left\langle \nabla \hat{f}_n(X_i) - \nabla f^*(X_i), X_i^j(e_j - X_i) \right\rangle \right| \\
&\leq \frac{1}{n} \sum_{i=1}^n \left| \left\langle \nabla \hat{f}_n(X_i) - \nabla f^*(X_i), X_i^j(e_j - X_i) \right\rangle \right| \\
&\leq \frac{1}{n} \sum_{i=1}^n \left\| \nabla \hat{f}_n(X_i) - \nabla f^*(X_i) \right\|_2 \left\| X_i^j(e_j - X_i) \right\|_2 \\
&\leq \frac{1}{n} \sum_{i=1}^n \left\| \nabla \hat{f}_n(X_i) - \nabla f^*(X_i) \right\|_2,
\end{aligned}$$

where for the last three steps we used the triangle inequality, the Cauchy-Schwartz inequality and that $\|X_i^j(e_j - X_i)\|_2 \leq 1$ since $X_i \in \mathbb{S}^{p-1}$, respectively. By assumption, it therefore holds that $A_n \rightarrow 0$ in probability as $n \rightarrow \infty$. For the B_n term, observe that using the same bounds it holds that

$$\mathbb{E} \left[\left(\frac{d}{dc} f^*(\psi(X_i, c)|_{c=1}) \right)^2 \right] = \mathbb{E} \left[\left(\left\langle \nabla f^*(X_i), X_i^j(e_j - X_i) \right\rangle \right)^2 \right] \leq \mathbb{E} \left[\left\| \nabla f^*(X_i) \right\|_2^2 \right].$$

By assumption that $\mathbb{E} \left[\left\| \nabla f^*(X_i) \right\|_2^2 \right] < \infty$ this implies we can apply the weak law of large numbers to get for $n \rightarrow \infty$ that

$$\hat{I}_{f^*}^j = \frac{1}{n} \sum_{i=1}^n \frac{d}{dc} f^*(\psi(X_i, c)|_{c=1}) \xrightarrow{P} \mathbb{E} \left[\frac{d}{dc} f^*(\psi(X_i, c)|_{c=1}) \right] = I_{f^*}^j.$$

This immediately implies that $B_n \rightarrow 0$ in probability as $n \rightarrow \infty$. Combining the convergence of A_n and B_n in (18) completes the proof of (i).

Next, we prove (ii). Fix $j \in \{1, \dots, p\}$ and $z \in [0, 1]$ such that $z/(1-z) \in \text{supp}(X^j / \sum_{\ell \neq j} X^\ell)$. By the definition of the perturbation ϕ_j we get that

$$\phi_j(X, z) = s(X^1, \dots, X^{j-1}, \frac{z}{1-z} \sum_{\ell \neq j} X^\ell, X^{j+1}, \dots, X^p) \quad (19)$$

where $s = (1-z)/(\sum_{\ell \neq j} X^\ell)$. Next, using the assumption that $\text{supp}(X) = \{x \in \mathbb{S}^{p-1} \mid x = w/(\sum_j w^j) \text{ with } w \in \text{supp}(X^1) \times \dots \times \text{supp}(X^p)\}$ and that $z/(1-z) \in \text{supp}(X^j / \sum_{\ell \neq j} X^\ell)$ we get that

$$\phi_j(X, z) \in \text{supp}(X^j) \quad (20)$$

almost surely.

By the triangle inequality it holds that

$$|\hat{S}_{\hat{f}_n}^j(z) - S_{f^*}^j(z)| \leq \underbrace{|\hat{S}_{\hat{f}_n}^j(z) - \hat{S}_{f^*}^j(z)|}_{=:C_n} + \underbrace{|\hat{S}_{f^*}^j(z) - S_{f^*}^j(z)|}_{=:D_n}. \quad (21)$$

We now consider the two terms C_n and D_n separately. First, we apply the triangle inequality to bound the C_n term as follows.

$$\begin{aligned} C_n &= \left| \frac{1}{n} \sum_{i=1}^n (\hat{f}_n(\phi_j(X_i, z)) - f^*(\phi_j(X_i, z))) + \frac{1}{n} \sum_{i=1}^n (\hat{f}_n(X_i) - f^*(X_i)) \right| \\ &\leq \frac{1}{n} \sum_{i=1}^n \left| \hat{f}_n(\phi_j(X_i, z)) - f^*(\phi_j(X_i, z)) \right| + \frac{1}{n} \sum_{i=1}^n \left| \hat{f}_n(X_i) - f^*(X_i) \right| \\ &\leq 2 \sup_{x \in \text{supp}(X)} \left| \hat{f}_n(x) - f^*(x) \right|, \end{aligned}$$

where for the last step we used a supremum bound together with (19). Hence, using the assumption that $\sup_{x \in \text{supp}(X)} |\hat{f}_n(x) - f^*(x)| \xrightarrow{P} 0$ as $n \rightarrow \infty$, we get that $C_n \rightarrow 0$ in probability as $n \rightarrow \infty$. Similarly, for the D_n term we get that

$$\begin{aligned} D_n &= \left| \frac{1}{n} \sum_{i=1}^n f^*(\phi_j(X_i, z)) - \mathbb{E}[f^*(\phi_j(X_i, z))] + \frac{1}{n} \sum_{i=1}^n f^*(X_i) - \mathbb{E}[f^*(X_i)] \right| \\ &\leq \left| \frac{1}{n} \sum_{i=1}^n f^*(\phi_j(X_i, z)) - \mathbb{E}[f^*(\phi_j(X_i, z))] \right| + \left| \frac{1}{n} \sum_{i=1}^n f^*(X_i) - \mathbb{E}[f^*(X_i)] \right|. \end{aligned}$$

Since the X_1, \dots, X_n and hence $\phi_j(X_1, z), \dots, \phi_j(X_n, z)$ are i.i.d. and bounded we can apply the weak law of large numbers to get that $D_n \rightarrow 0$ in probability as $n \rightarrow \infty$.

Finally, combining the convergence of C_n and D_n with (21) proves (ii) and hence completes the proof of Theorem 2.1. \square

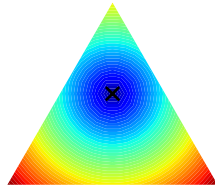
G List of kernels implemented in KernelBiome

In this section we summarize the all kernels implemented in `KernelBiome` and visualize the metrics and kernels via heatmaps when $p = 3$. The reference points are the neutral point $u = (\frac{1}{3}, \frac{1}{3}, \frac{1}{3})$, a vertex $v = (1, 0, 0)$, a midpoint on a boundary $m = (\frac{1}{2}, \frac{1}{2}, 0)$, and an interior point $z = (\frac{1}{4}, \frac{1}{4}, \frac{1}{2})$ of the simplex. For kernels we omit the neutral point, since $k(x, u) = 0$ for any $x \in \mathbb{S}^2$, as we centered our kernels at u .

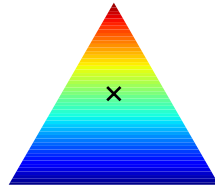
Linear metric & kernel

$$d^2(x, y) = \sum_{j=1}^p (x^j - y^j)^2$$

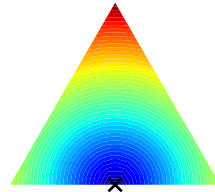
$$k(x, y) = \left(\sum_{j=1}^p x^j y^j \right) - \frac{1}{p}$$



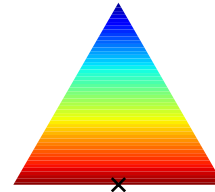
$d(x, z)$



$k(x, z)$



$d(x, m)$

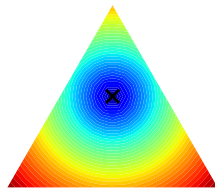


$k(x, m)$

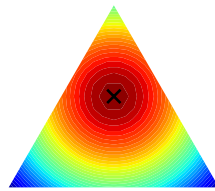
RBF metric & kernel

$$d^2(x, y) = 2 - 2 \exp \left(- \sum_{j=1}^p \frac{(x^j - y^j)^2}{2\sigma^2} \right)$$

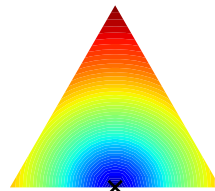
$$k(x, y) = \exp \left(- \sum_{j=1}^p \frac{(x^j - y^j)^2}{2\sigma^2} \right)$$



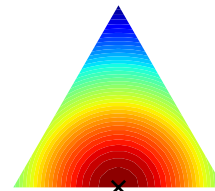
$d_{\sigma=\frac{1}{\sqrt{2}}}(x, z)$



$k_{\sigma=\frac{1}{\sqrt{2}}}(x, z)$



$d_{\sigma=\frac{1}{\sqrt{2}}}(x, m)$

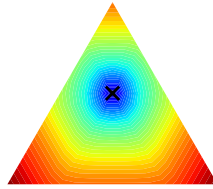


$k_{\sigma=\frac{1}{\sqrt{2}}}(x, m)$

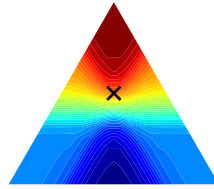
Generalized-JS metric & kernel ($a < \infty, b \in [0.5, a)$)

$$d^2(x, y) = \frac{ab}{a-b} \sum_{j=1}^p \frac{2^{\frac{1}{b}} \left[(x^j)^a + (y^j)^a \right]^{\frac{1}{a}} - 2^{\frac{1}{a}} \left[(x^j)^b + (y^j)^b \right]^{\frac{1}{b}}}{2^{\frac{1}{a} + \frac{1}{b}}}$$

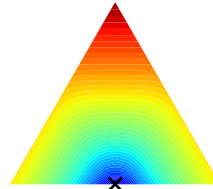
$$k(x, y) = -\frac{ab}{a-b} \cdot 2^{-(1+\frac{1}{a}+\frac{1}{b})} \sum_{j=1}^p \left\{ 2^{\frac{1}{b}} \left(\left[(x^j)^a + (y^j)^a \right]^{\frac{1}{a}} - \left[(x^j)^a + \left(\frac{1}{p}\right)^a \right]^{\frac{1}{a}} \right. \right. \\ \left. \left. - \left[\left(\frac{1}{p}\right)^a + (y^j)^a \right]^{\frac{1}{a}} \right) - 2^{\frac{1}{a}} \left(\left[(x^j)^b + (y^j)^b \right]^{\frac{1}{b}} - \left[(x^j)^b + \left(\frac{1}{p}\right)^b \right]^{\frac{1}{b}} \right. \right. \\ \left. \left. - \left[\left(\frac{1}{p}\right)^b + (y^j)^b \right]^{\frac{1}{b}} \right) \right\}$$



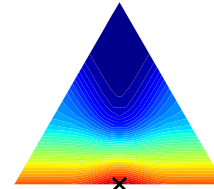
$d_{a=10, b=1}(x, z)$



$k_{a=10, b=1}(x, z)$



$d_{a=10, b=1}(x, m)$

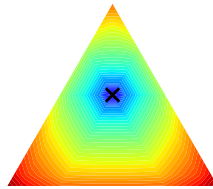


$k_{a=10, b=1}(x, m)$

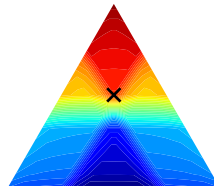
Generalized-JS metric & kernel ($a \rightarrow \infty, b < \infty$)

$$d^2(x, y) = \sum_{j=1}^p b \left\{ 2^{\frac{1}{b}} \cdot \max\{x^j, y^j\} - \left[(x^j)^b + (y^j)^b \right]^{\frac{1}{b}} \right\}$$

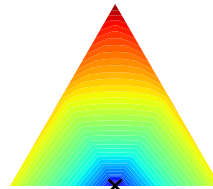
$$k(x, y) = -\frac{b}{2} \sum_{j=1}^p \left\{ 2^{\frac{1}{b}} \left(\max\{x^j, y^j\} - \max\{x^j, \frac{1}{p}\} - \max\{y^j, \frac{1}{p}\} \right) \right. \\ \left. - \left[(x^j)^b + (y^j)^b \right]^{\frac{1}{b}} + \left[(x^j)^b + \left(\frac{1}{p}\right)^b \right]^{\frac{1}{b}} + \left[(y^j)^b + \left(\frac{1}{p}\right)^b \right]^{\frac{1}{b}} \right\}$$



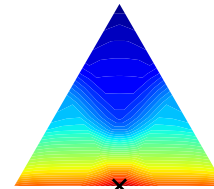
$d_{a=\infty, b=0.5}(x, z)$



$k_{a=\infty, b=0.5}(x, z)$



$d_{a=\infty, b=0.5}(x, m)$

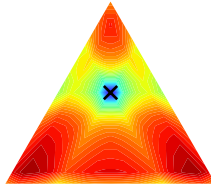


$k_{a=\infty, b=0.5}(x, m)$

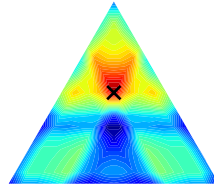
Generalized-JS metric & kernel ($a < \infty, b \rightarrow a$)

$$d^2(x, y) = \sum_{j=1}^p \left[\frac{(x^j)^b + (y^j)^b}{2} \right]^{\frac{1}{b}} \cdot \left[\frac{(x^j)^b}{(x^j)^b + (y^j)^b} \cdot \log \frac{2(x^j)^b}{(x^j)^b + (y^j)^b} \right. \\ \left. + \frac{(y^j)^b}{(x^j)^b + (y^j)^b} \cdot \log \frac{2(y^j)^b}{(x^j)^b + (y^j)^b} \right]$$

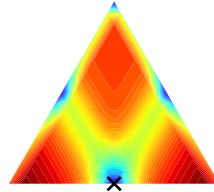
$$k(x, y) = -\frac{1}{2^{\frac{1}{b}+1}} \sum_{j=1}^p \left\{ \left[(x^j)^b + (y^j)^b \right]^{\frac{1}{b}-1} \cdot \left((x^j)^b \cdot \log \left[2(x^j)^b \right] + (y^j)^b \log \left[2(y^j)^b \right] \right. \right. \\ \left. - \left[(x^j)^b + (y^j)^b \right] \cdot \log \left[(x^j)^b + (y^j)^b \right] \right) \\ - \left[(x^j)^b + \frac{1}{p^b} \right]^{\frac{1}{b}-1} \cdot \left(- \left[(x^j)^b + \left(\frac{1}{p^b} \right) \right] \cdot \log \left[(x^j)^b + \frac{1}{p^b} \right] \right. \\ \left. + (x^j)^b \cdot \log \left[2(x^j)^b \right] + \frac{1}{p^b} \cdot \log \left[\frac{2}{p^b} \right] \right) \\ - \left[(y^j)^b + \frac{1}{p^b} \right]^{\frac{1}{b}-1} \cdot \left(- \left[(y^j)^b + \left(\frac{1}{p^b} \right) \right] \cdot \log \left[(y^j)^b + \frac{1}{p^b} \right] \right. \\ \left. + (y^j)^b \cdot \log \left[2(y^j)^b \right] + \frac{1}{p^b} \cdot \log \left[\frac{2}{p^b} \right] \right) \right\}$$



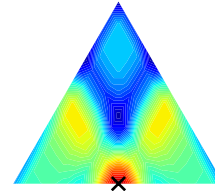
$d_{a=b=10}(x, z)$



$k_{a=b=10}(x, z)$



$d_{a=b=10}(x, m)$

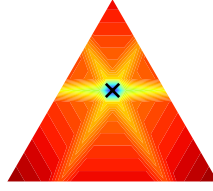


$k_{a=b=10}(x, m)$

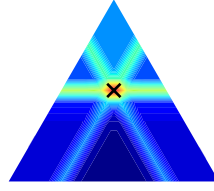
Generalized-JS metric & kernel ($a = b \rightarrow \infty$)

$$d^2(x, y) = \sum_{j=1}^p \max\{x^j, y^j\} \cdot \left[\log(2) \mathbb{1}\{x^j \neq y^j\} \right]$$

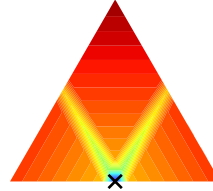
$$k(x, y) = -\frac{\log(2)}{2} \cdot \sum_{j=1}^p \left\{ \max\{x^j, y^j\} \cdot \mathbb{1}\{x^j \neq y^j\} \right. \\ \left. - \max\{x^j, \frac{1}{p}\} \cdot \mathbb{1}\{x^j \neq \frac{1}{p}\} - \max\{y^j, \frac{1}{p}\} \cdot \mathbb{1}\{y^j \neq \frac{1}{p}\} \right\}$$



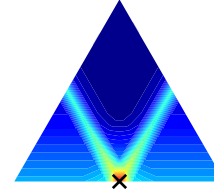
$d_{a=b=\infty}(x, z)$



$k_{a=b=\infty}(x, z)$



$d_{a=b=\infty}(x, m)$



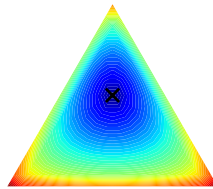
$k_{a=b=\infty}(x, m)$

Speical Case: Hellinger - Generalized-JS metric & kernel ($a = 1, b = \frac{1}{2}$)

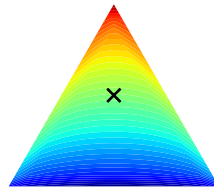
$$d^2(x, y) = \frac{\sqrt{2}}{2} \sum_{j=1}^p (\sqrt{x^j} - \sqrt{y^j})^2$$

$$k(x, y) = \frac{\sqrt{2}}{4} + \frac{\sqrt{2}}{4} \sum_{j=1}^p \left\{ \sqrt{x^j y^j} - \frac{\sqrt{x^j} + \sqrt{y^j}}{\sqrt{p}} \right\}$$

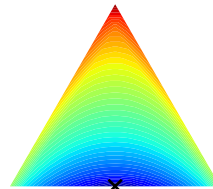
This corresponds to $\frac{\sqrt{2}}{2}$ times the **Hellinger** metric and kernel.



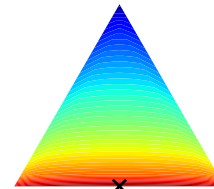
$d_{a=1,b=0.5}(x, z)$



$k_{a=1,b=0.5}(x, z)$



$d_{a=1,b=0.5}(x, m)$



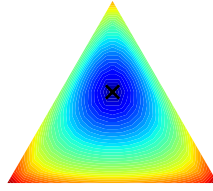
$k_{a=1,b=0.5}(x, m)$

Special Case: Jenson-Shannon - Generalized-JS metric & kernel ($a = 1, b = 1$)

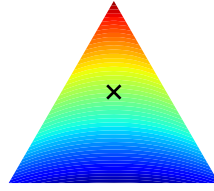
$$d^2(x, y) = \frac{1}{2} \sum_{j=1}^p x^j \log \frac{2x^j}{x^j + y^j} + y^j \log \frac{2y^j}{x^j + y^j}$$

$$k(x, y) = -\frac{1}{4} \sum_{j=1}^p \left\{ x^j \log \frac{x^j + \frac{1}{p}}{x^j + y^j} + y^j \log \frac{y^j + \frac{1}{p}}{x^j + y^j} - \frac{1}{p} \log \frac{4}{p^2(x^j + \frac{1}{p})(y^j + \frac{1}{p})} \right\}$$

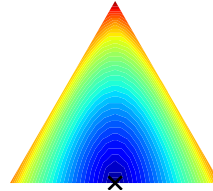
This corresponds to the **Jenson-Shannon** metric and kernel.



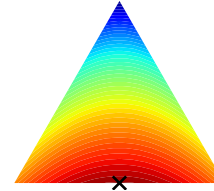
$d_{a=b=1}(x, z)$



$k_{a=b=1}(x, z)$



$d_{a=b=1}(x, z)$



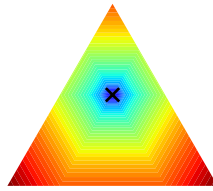
$k_{a=b=1}(x, z)$

Special Case: Total Variation - Generalized-JS metric & kernel ($a = \infty, b = 1$)

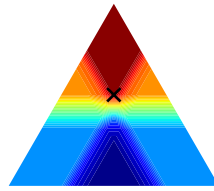
$$d^2(x, y) = \sum_{j=1}^p |x^j - y^j|$$

$$k(x, y) = -\frac{1}{2} \sum_{j=1}^p \left\{ |x^j - y^j| - |x^j - \frac{1}{p}| - |y^j - \frac{1}{p}| \right\}$$

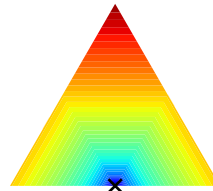
This corresponds to 2 times the **total variation** metric and kernel.



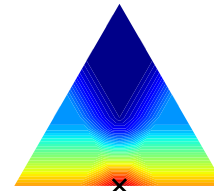
$d_{a=\infty, b=1}(x, z)$



$k_{a=\infty, b=1}(x, z)$



$d_{a=\infty, b=1}(x, z)$

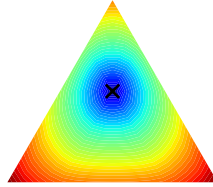


$k_{a=\infty, b=1}(x, z)$

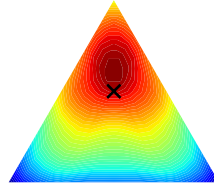
Hilbertian metric & kernel ($a < \infty, b > -\infty$)

$$d^2(x, y) = \sum_{j=1}^p \frac{2^{\frac{1}{b}} \left[(x^j)^a + (y^j)^a \right]^{\frac{1}{a}} - 2^{\frac{1}{a}} \left[(x^j)^b + (y^j)^b \right]^{\frac{1}{b}}}{2^{\frac{1}{a}} - 2^{\frac{1}{b}}}$$

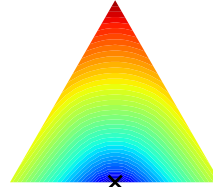
$$k(x, y) = -\frac{1}{2(2^{\frac{1}{a}} - 2^{\frac{1}{b}})} \sum_{j=1}^p \left\{ 2^{\frac{1}{b}} \left(\left[(x^j)^a + (y^j)^a \right]^{\frac{1}{a}} - \left[(x^j)^a + \left(\frac{1}{p}\right)^a \right]^{\frac{1}{a}} \right. \right. \\ \left. \left. - \left[(y^j)^a + \left(\frac{1}{p}\right)^a \right]^{\frac{1}{a}} \right) - 2^{\frac{1}{a}} \left(\left[(x^j)^b + (y^j)^b \right]^{\frac{1}{b}} - \left[(x^j)^b + \left(\frac{1}{p}\right)^b \right]^{\frac{1}{b}} \right. \right. \\ \left. \left. - \left[(y^j)^b + \left(\frac{1}{p}\right)^b \right]^{\frac{1}{b}} \right) \right\}$$



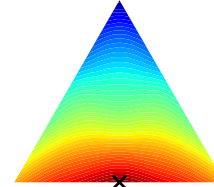
$d_{a=10, b=-1}(x, z)$



$k_{a=10, b=-1}(x, z)$



$d_{a=10, b=-1}(x, m)$

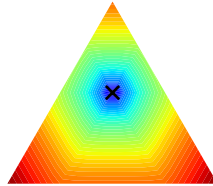


$k_{a=10, b=-1}(x, m)$

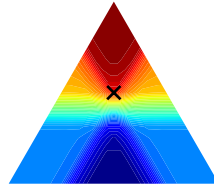
Hilbertian metric & kernel ($a \rightarrow \infty, b > -\infty$)

$$d^2(x, y) = \sum_{j=1}^p b \left\{ 2^{\frac{1}{b}} \cdot \max\{x^j, y^j\} - \left[(x^j)^b + (y^j)^b \right]^{\frac{1}{b}} \right\}$$

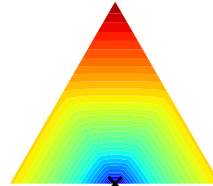
$$k(x, y) = -\frac{1}{2(1 - 2^{\frac{1}{b}})} \sum_{j=1}^p \left\{ 2^{\frac{1}{b}} \left(\max\{x^j, y^j\} - \max\{x^j, \frac{1}{p}\} - \max\{y^j, \frac{1}{p}\} \right) \right. \\ \left. - \left[(x^j)^b + (y^j)^b \right]^{\frac{1}{b}} + \left[(x^j)^b + \left(\frac{1}{p}\right)^b \right]^{\frac{1}{b}} + \left[(y^j)^b + \left(\frac{1}{p}\right)^b \right]^{\frac{1}{b}} \right\}$$



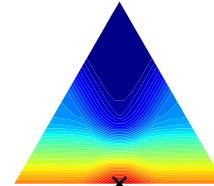
$d_{a=\infty, b=-10}(x, z)$



$k_{a=\infty, b=-10}(x, z)$



$d_{a=\infty, b=-10}(x, m)$

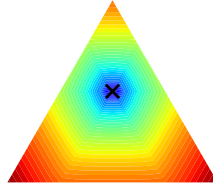


$k_{a=\infty, b=-10}(x, m)$

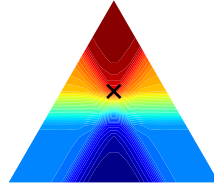
Hilbertian metric & kernel ($a < \infty, b \rightarrow -\infty$)

$$d^2(x, y) = \frac{1}{2^{\frac{1}{a}} - 1} \sum_{j=1}^p \left\{ \left[(x^j)^a + (y^j)^a \right]^{\frac{1}{a}} - 2^{\frac{1}{a}} \cdot \min\{x^j, y^j\} \right\}$$

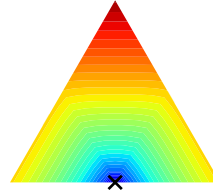
$$k(x, y) = -\frac{1}{2(2^{\frac{1}{a}} - 1)} \sum_{j=1}^p \left\{ \left[(x^j)^a + (y^j)^a \right]^{\frac{1}{a}} - \left[(x^j)^a + \left(\frac{1}{p}\right)^a \right]^{\frac{1}{a}} - \left[(y^j)^a + \left(\frac{1}{p}\right)^a \right]^{\frac{1}{a}} \right. \\ \left. - 2^{\frac{1}{a}} \left[\min\{x^j, y^j\} - \min\{x^j, \frac{1}{p}\} - \min\{y^j, \frac{1}{p}\} \right] \right\}$$



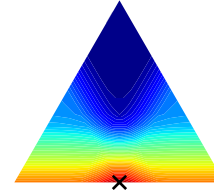
$d_{a=10, b=-\infty}(x, z)$



$k_{a=10, b=-\infty}(x, z)$



$d_{a=10, b=-\infty}(x, m)$



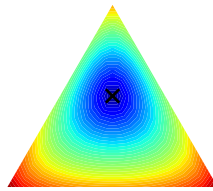
$k_{a=10, b=-\infty}(x, m)$

Special Case: Chi-square - Hilbertian metric & kernel ($a = 1, b = -1$)

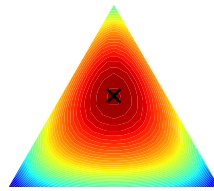
$$d^2(x, y) = \frac{1}{3} \sum_{j=1}^p \frac{(x^j - y^j)^2}{x^j + y^j}$$

$$k(x, y) = -\frac{1}{6} \sum_{j=1}^p \left\{ \frac{(x^j - y^j)^2}{x^j + y^j} - \frac{(x^j - \frac{1}{p})^2}{x^j + \frac{1}{p}} - \frac{(y^j - \frac{1}{p})^2}{y^j + \frac{1}{p}} \right\}$$

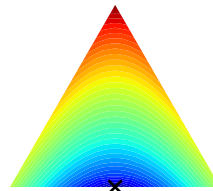
This corresponds to $\frac{1}{3}$ of the **chi-square** metric and kernel.



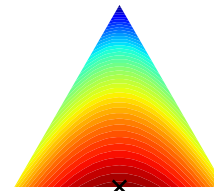
$d_{a=1, b=-1}(x, z)$



$k_{a=1, b=-1}(x, z)$



$d_{a=1, b=-1}(x, m)$



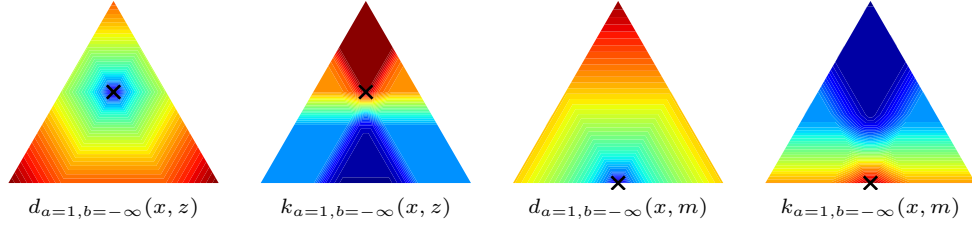
$k_{a=1, b=-1}(x, m)$

Special Case: Total Variation - Hilbertian metric & kernel ($a = 1, b = -\infty$)

$$d^2(x, y) = \frac{1}{2} \sum_{j=1}^p |x^j - y^j|$$

$$k(x, y) = -\frac{1}{4} \sum_{j=1}^p \left\{ |x^j - y^j| - \left| x^j - \frac{1}{p} \right| - \left| y^j - \frac{1}{p} \right| \right\}$$

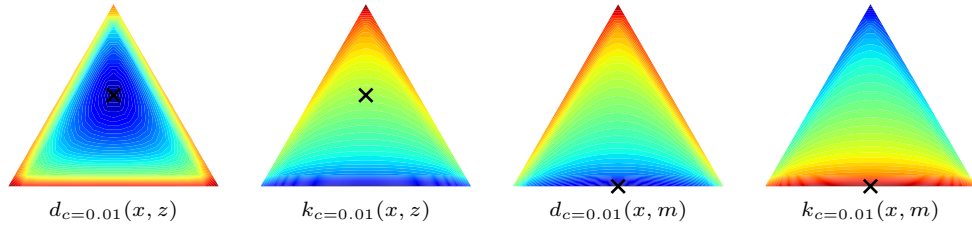
This corresponds to the **total variation** metric and kernel.



Aitchison metric & kernel

$$d^2(x, y) = \sum_{j=1}^p \left(\log \frac{x^j + c}{g(x + c)} - \log \frac{y^j + c}{g(y + c)} \right)^2$$

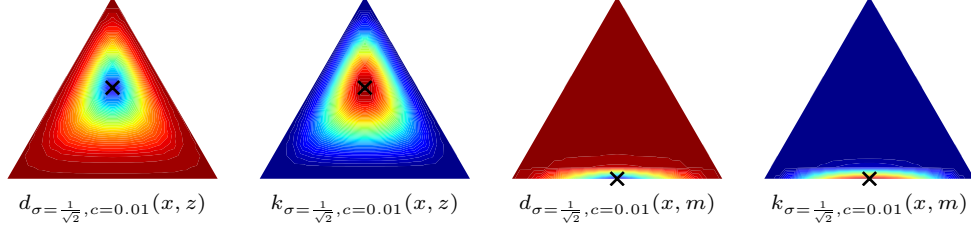
$$k(x, y) = \sum_{j=1}^p \log \frac{x^j + c}{g(x + c)} \log \frac{y^j + c}{g(y + c)}$$



Aitchison-RBF metric & kernel

$$d^2(x, y) = 2 - 2 \exp \left(- \frac{1}{2\sigma^2} \sum_{j=1}^p \left[\log \frac{x^j + c}{g(x+c)} - \log \frac{y^j + c}{g(y+c)} \right]^2 \right)$$

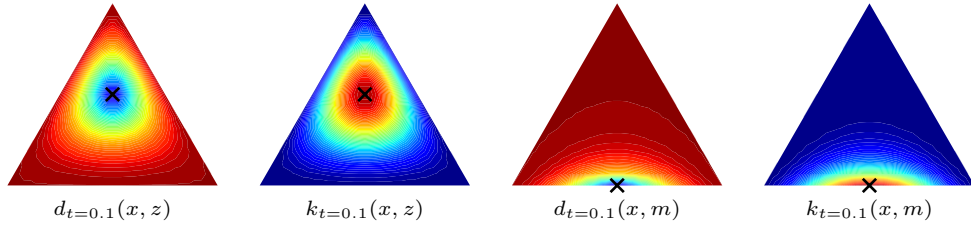
$$k(x, y) = \exp \left(- \frac{1}{2\sigma^2} \sum_{j=1}^p \left[\log \frac{x^j + c}{g(x+c)} - \log \frac{y^j + c}{g(y+c)} \right]^2 \right)$$



Heat diffusion metric & kernel

$$d^2(x, y) = 2 \cdot (4\pi t)^{-\frac{p}{2}} \cdot \left[1 - \exp \left(- \frac{1}{t} \arccos^2 \left(\sum_{j=1}^p \sqrt{x^j y^j} \right) \right) \right]$$

$$k(x, y) = (4\pi t)^{-p/2} \cdot \exp \left(- \frac{1}{t} \arccos^2 \left(\sum_{j=1}^p \sqrt{x^j y^j} \right) \right)$$



G.1 List of weighted kernels

As discussed in Section B, all kernels can also be modified to include a weight matrix $W \in \mathbb{R}^{p \times p}$. Below, we list the explicit forms of all weighted kernels as they are implemented in KernelBiome package.

Linear kernel

$$k(x, y) = \sum_{j, \ell=1}^p W_{j, \ell} \left(x^j y^\ell - \frac{x^j}{p} - \frac{y^\ell}{p} + \frac{1}{p^2} \right)$$

RBF kernel

$$k(x, y) = \exp \left(- \sum_{j, \ell=1}^p \frac{W_{j, \ell} (x^j - y^\ell)^2}{2\sigma^2} \right)$$

Generalized-JS kernel ($a < \infty, b \in [0.5, a]$)

$$\begin{aligned} k(x, y) = & -\frac{ab}{a-b} \cdot 2^{-(1+\frac{1}{a}+\frac{1}{b})} \sum_{j, \ell=1}^p W_{j, \ell} \left\{ 2^{\frac{1}{b}} \left(\left[(x^j)^a + (y^\ell)^a \right]^{\frac{1}{a}} - \left[(x^j)^a + \left(\frac{1}{p} \right)^a \right]^{\frac{1}{a}} \right. \right. \\ & - \left. \left[\left(\frac{1}{p} \right)^a + (y^\ell)^a \right]^{\frac{1}{a}} \right) - 2^{\frac{1}{a}} \left(\left[(x^j)^b + (y^\ell)^b \right]^{\frac{1}{b}} - \left[(x^j)^b + \left(\frac{1}{p} \right)^b \right]^{\frac{1}{b}} \right. \\ & \left. \left. - \left[\left(\frac{1}{p} \right)^b + (y^\ell)^b \right]^{\frac{1}{b}} \right) \right\} \end{aligned}$$

Generalized-JS kernel ($a \rightarrow \infty, b < \infty$)

$$\begin{aligned} k(x, y) = & -\frac{b}{2} \sum_{j, \ell=1}^p W_{j, \ell} \left\{ 2^{\frac{1}{b}} \left(\max\{x^j, y^\ell\} - \max\{x^j, \frac{1}{p}\} - \max\{y^\ell, \frac{1}{p}\} \right) \right. \\ & \left. - \left[(x^j)^b + (y^\ell)^b \right]^{\frac{1}{b}} + \left[(x^j)^b + \left(\frac{1}{p} \right)^b \right]^{\frac{1}{b}} + \left[(y^\ell)^b + \left(\frac{1}{p} \right)^b \right]^{\frac{1}{b}} \right\} \end{aligned}$$

Generalized-JS kernel ($a < \infty, b \rightarrow a$)

$$\begin{aligned} k(x, y) = & -\frac{1}{2^{\frac{1}{b}+1}} \sum_{j, \ell=1}^p W_{j, \ell} \left\{ \left[(x^j)^b + (y^\ell)^b \right]^{\frac{1}{b}-1} \cdot \left((x^j)^b \cdot \log \left[2(x^j)^b \right] + (y^\ell)^b \log \left[2(y^\ell)^b \right] \right. \right. \\ & - \left. \left[(x^j)^b + (y^\ell)^b \right] \cdot \log \left[(x^j)^b + (y^\ell)^b \right] \right) \\ & - \left[(x^j)^b + \frac{1}{p^b} \right]^{\frac{1}{b}-1} \cdot \left(- \left[(x^j)^b + \left(\frac{1}{p^b} \right) \right] \cdot \log \left[(x^j)^b + \frac{1}{p^b} \right] + (x^j)^b \cdot \log \left[2(x^j)^b \right] + \frac{1}{p^b} \cdot \log \left[\frac{2}{p^b} \right] \right) \\ & \left. - \left[(y^\ell)^b + \frac{1}{p^b} \right]^{\frac{1}{b}-1} \cdot \left(- \left[(y^\ell)^b + \left(\frac{1}{p^b} \right) \right] \cdot \log \left[(y^\ell)^b + \frac{1}{p^b} \right] + (y^\ell)^b \cdot \log \left[2(y^\ell)^b \right] + \frac{1}{p^b} \cdot \log \left[\frac{2}{p^b} \right] \right) \right\} \end{aligned}$$

Generalized-JS kernel ($a = b \rightarrow \infty$)

$$\begin{aligned} k(x, y) = & -\frac{\log(2)}{2} \cdot \sum_{j, \ell=1}^p W_{j, \ell} \left\{ \max\{x^j, y^\ell\} \cdot \mathbb{1}\{x^j \neq y^\ell\} \right. \\ & \left. - \max\{x^j, \frac{1}{p}\} \cdot \mathbb{1}\{x^j \neq \frac{1}{p}\} - \max\{y^\ell, \frac{1}{p}\} \cdot \mathbb{1}\{y^\ell \neq \frac{1}{p}\} \right\} \end{aligned}$$

Hilbertian kernel ($a < \infty, b > -\infty$)

$$k(x, y) = -\frac{1}{2(2^{\frac{1}{a}} - 2^{\frac{1}{b}})} \sum_{j,\ell=1}^p W_{j,\ell} \left\{ 2^{\frac{1}{b}} \left(\left[(x^j)^a + (y^\ell)^a \right]^{\frac{1}{a}} - \left[(x^j)^a + \left(\frac{1}{p}\right)^a \right]^{\frac{1}{a}} \right. \right. \\ \left. \left. - \left[(y^\ell)^a + \left(\frac{1}{p}\right)^a \right]^{\frac{1}{a}} \right) - 2^{\frac{1}{a}} \left(\left[(x^j)^b + (y^\ell)^b \right]^{\frac{1}{b}} - \left[(x^j)^b + \left(\frac{1}{p}\right)^b \right]^{\frac{1}{b}} \right. \right. \\ \left. \left. - \left[(y^\ell)^b + \left(\frac{1}{p}\right)^b \right]^{\frac{1}{b}} \right) \right\}$$

Hilbertian kernel ($a \rightarrow \infty, b > -\infty$)

$$k(x, y) = -\frac{1}{2(1 - 2^{\frac{1}{b}})} \sum_{j,\ell=1}^p W_{j,\ell} \left\{ 2^{\frac{1}{b}} \left(\max\{x^j, y^\ell\} - \max\{x^j, \frac{1}{p}\} - \max\{y^\ell, \frac{1}{p}\} \right) \right. \\ \left. - \left[(x^j)^b + (y^\ell)^b \right]^{\frac{1}{b}} + \left[(x^j)^b + \left(\frac{1}{p}\right)^b \right]^{\frac{1}{b}} + \left[(y^\ell)^b + \left(\frac{1}{p}\right)^b \right]^{\frac{1}{b}} \right\}$$

Hilbertian kernel ($a < \infty, b \rightarrow -\infty$)

$$k(x, y) = -\frac{1}{2(2^{\frac{1}{a}} - 1)} \sum_{j,\ell=1}^p W_{j,\ell} \left\{ \left[(x^j)^a + (y^\ell)^a \right]^{\frac{1}{a}} - \left[(x^j)^a + \left(\frac{1}{p}\right)^a \right]^{\frac{1}{a}} - \left[(y^\ell)^a + \left(\frac{1}{p}\right)^a \right]^{\frac{1}{a}} \right. \\ \left. - 2^{\frac{1}{a}} \left[\min\{x^j, y^\ell\} - \min\{x^j, \frac{1}{p}\} - \min\{y^\ell, \frac{1}{p}\} \right] \right\}$$

Aitchison kernel

$$k(x, y) = \sum_{j,\ell=1}^p W_{j,\ell} \log \frac{x^j + c}{g(x + c)} \log \frac{y^\ell + c}{g(y + c)}$$

Aitchison RBF kernel

$$k(x, y) = \exp \left(-\frac{1}{2\sigma^2} \sum_{j,\ell=1}^p W_{j,\ell} \left[\log \frac{x^j + c}{g(x + c)} - \log \frac{y^\ell + c}{g(y + c)} \right]^2 \right)$$

Heat diffusion kernel

$$k(x, y) = (4\pi t)^{-p/2} \cdot \exp \left(-\frac{1}{t} \arccos^2 \left(\sum_{j,\ell=1}^p W_{j,\ell} \sqrt{x^j y^\ell} \right) \right)$$

References

- Elisabeth Ailer, Christian L Müller, and Niki Kilbertus. A causal view on compositional data. *arXiv preprint arXiv:2106.11234*, 2021.
- J. Aitchison. Principal component analysis of compositional data. *Biometrika*, 70(1):57–65, 04 1983. ISSN 0006-3444. doi: 10.1093/biomet/70.1.57. URL <https://doi.org/10.1093/biomet/70.1.57>.
- John Aitchison. The statistical analysis of compositional data. *Journal of the Royal Statistical Society: Series B (Methodological)*, 44(2):139–160, 1982.
- John Aitchison. A general class of distributions on the simplex. *Journal of the Royal Statistical Society: Series B (Methodological)*, 47(1):136–146, 1985.
- John Aitchison and John Bacon-Shone. Log contrast models for experiments with mixtures. *Biometrika*, 71(2):323–330, 1984. ISSN 00063444. doi: 10.1093/biomet/71.2.323.
- John Aitchison and Michael Greenacre. Biplots of compositional data. *Journal of the Royal Statistical Society: Series C (Applied Statistics)*, 51(4):375–392, 2002. doi: <https://doi.org/10.1111/1467-9876.00275>. URL <https://rss.onlinelibrary.wiley.com/doi/abs/10.1111/1467-9876.00275>.
- J. Bradbury, R. Frostig, P. Hawkins, M. J. Johnson, C. Leary, D. Maclaurin, G. Necula, A. Paszke, J. VanderPlas, S. Wanderman-Milne, and Q. Zhang. JAX: composable transformations of Python+NumPy programs, 2018. <http://github.com/google/jax>.
- Antonella Buccianti, Glòria Mateu-Figueras, and Vera Pawlowsky-Glahn. Compositional data analysis in the geosciences: from theory to practice. In *GSL Special Publications*. Geological Society of London, 2006.
- G. Cammarota, G. Ianaro, A. Ahern, C. Carbone, A. Temko, M. J. Claesson, A. Gasbarrini, and G. Tortora. Gut microbiome, big data and machine learning to promote precision medicine for cancer. *Nature reviews gastroenterology & hepatology*, 17(10):635–648, 2020.
- Anne Chao, Chun-Huo Chiu, and Lou Jost. Unifying species diversity, phylogenetic diversity, functional diversity, and related similarity and differentiation measures through hill numbers. *Annual review of ecology, evolution, and systematics*, 45:297–324, 2014.
- Jun Chen and Hongzhe Li. Kernel methods for regression analysis of microbiome compositional data. In *Topics in Applied Statistics*, pages 191–201. Springer, 2013.
- Aisling J Daly, Jan M Baetens, and Bernard De Baets. Ecological diversity: measuring the unmeasurable. *Mathematics*, 6(7):119, 2018.

- Marco Di Marzio, Agnese Panzera, and Catia Venieri. Non-parametric regression for compositional data. *Statistical Modelling*, 15(2):113–133, 2015.
- Carl Eckart and Gale Young. The approximation of one matrix by another of lower rank. *Psychometrika*, 1(3):211–218, 1936.
- Juan José Egozcue, Vera Pawlowsky-Glahn, Glòria Mateu-Figueras, and Carles Barcelo-Vidal. Isometric logratio transformations for compositional data analysis. *Mathematical Geology*, 35(3):279–300, 2003.
- Andrew D Fernandes, Jean M Macklaim, Thomas G Linn, Gregor Reid, and Gregory B Gloor. Anova-like differential expression (aldex) analysis for mixed population rna-seq. *PloS one*, 8(7):e67019, 2013.
- J. H. Friedman. Greedy function approximation: a gradient boosting machine. *Annals of statistics*, pages 1189–1232, 2001.
- Jonathan Friedman and Eric J Alm. Inferring correlation networks from genomic survey data. *Computational Biology*, 2012.
- Gregory B Gloor, Jean M Macklaim, Vera Pawlowsky-Glahn, and Juan J Egozcue. Microbiome datasets are compositional: and this is not optional. *Frontiers in microbiology*, 8: 2224, 2017.
- W. Gou, C.-W. Ling, Y. He, Z. Jiang, Y. Fu, F. Xu, Z. Miao, T.-Y. Sun, J.-S. Lin, H.-L. Zhu, L. Zhou, Y.-M. Chen, and J.-S. Zheng. Interpretable machine learning framework reveals robust gut microbiome features associated with type 2 diabetes. *Diabetes Care*, 44(2):358–366, 2021.
- Matthias Hein and Olivier Bousquet. Hilbertian metrics and positive definite kernels on probability measures. In *International Workshop on Artificial Intelligence and Statistics*, pages 136–143. PMLR, 2005.
- G. Hooker, L. Mentch, and S. Zhou. Unrestricted permutation forces extrapolation: variable importance requires at least one more model, or there is no free variable importance. *Statistics and Computing*, 31(6):1–16, 2021.
- Donald A Jackson. Compositional data in community ecology: the paradigm or peril of proportions? *Ecology*, 78(3):929–940, 1997.
- Abhishek Kaul, Siddhartha Mandal, Ori Davidov, and Shyamal D Peddada. Analysis of microbiome data in the presence of excess zeros. *Frontiers in microbiology*, 8:2114, 2017.

- Rob Knight, Alison Vrbanc, Bryn C Taylor, Alexander Aksenov, Chris Callewaert, Justine Debelius, Antonio Gonzalez, Tomasz Kosciolk, Laura-Isobel McCall, Daniel McDonald, Alexey V. Melnik, James T. Morton, Jose Navas, Robert A. Quinn, Jon G. Sanders, Austin D. Swafford, Luke R. Thompson, Anupriya Tripathi, Zhenjiang Z. Xu, Jesse R. Zaneveld, Qiyun Zhu, J. Gregory Caporaso, and Pieter C. Dorrestein. Best practices for analysing microbiomes. *Nature Reviews Microbiology*, 16(7):410–422, 2018.
- I. E. Kumar, S. Venkatasubramanian, C. Scheidegger, and S. Friedler. Problems with shapley-value-based explanations as feature importance measures. In *International Conference on Machine Learning*, pages 5491–5500. PMLR, 2020.
- John Lafferty, Guy Lebanon, and Tommi Jaakkola. Diffusion kernels on statistical manifolds. *Journal of Machine Learning Research*, 6(1):129–163, 2005.
- Tom Leinster and Christina Cobbold. Measuring diversity: The importance of species similarity. *Ecology*, 93:477–89, 03 2012. doi: 10.2307/23143936.
- H. Li. Microbiome, metagenomics, and high-dimensional compositional data analysis. *Annual Review of Statistics and Its Application*, 2:73–94, 2015.
- Huang Lin and Shyamal Das Peddada. Analysis of microbial compositions: a review of normalization and differential abundance analysis. *NPJ biofilms and microbiomes*, 6(1): 1–13, 2020.
- Wei Lin, Pixu Shi, Rui Feng, and Hongzhe Li. Variable selection in regression with compositional covariates. *Biometrika*, 101(4):785–797, 08 2014. ISSN 0006-3444. doi: 10.1093/biomet/asu031. URL <https://doi.org/10.1093/biomet/asu031>.
- Catherine Lozupone and Rob Knight. Unifrac: a new phylogenetic method for comparing microbial communities. *Applied and environmental microbiology*, 71(12):8228–8235, 2005.
- Josep A Martín-Fernández, Carles Barceló-Vidal, and Vera Pawlowsky-Glahn. Dealing with zeros and missing values in compositional data sets using nonparametric imputation. *Mathematical Geology*, 35(3):253–278, 2003.
- C. Molnar. *Interpretable machine learning*. Lulu.com, 2020.
- F. Pedregosa, G. Varoquaux, A. Gramfort, V. Michel, B. Thirion, O. Grisel, M. Blondel, P. Prettenhofer, R. Weiss, V. Dubourg, J. Vanderplas, A. Passos, D. Cournapeau, M. Brucher, M. Perrot, and E. Duchesnay. Scikit-learn: Machine learning in Python. *Journal of Machine Learning Research*, 12:2825–2830, 2011.
- Misha Z Pesenson, Santosh K Suram, and John M Gregoire. Statistical analysis and interpolation of compositional data in materials science. *ACS combinatorial science*, 17(2):130–136, 2015.

- N. Qin, F. Yang, A. Li, E. Prifti, Y. Chen, L. Shao, J. Guo, E. Le Chatelier, J. Yao, L. Wu, J Zhou, S. Ni, L. Liu, N. Pons, J. M. Batto, S. P. Kennedy, P. Leonard, C. Yuan, W. Ding, Y Chen, X. Hu, B. Zheng, G. Qian, W. Xu, S. D. Ehrlich, S. Zheng, and L. Li. Alterations of the human gut microbiome in liver cirrhosis. *Nature*, 513(7516):59–64, 2014.
- Kelly S. Ramirez, Jonathan W. Leff, Albert Barberán, Scott Thomas Bates, Jason Betley, Thomas W. Crowther, Eugene F. Kelly, Emily E. Oldfield, E. Ashley Shaw, Christopher Steenbock, Mark A. Bradford, Diana H. Wall, and Noah Fierer. Biogeographic patterns in below-ground diversity in new york city’s central park are similar to those observed globally. *Proceedings of the royal society B: biological sciences*, 281(1795):20141988, 2014.
- Elies Ramon, Lluís Belanche-Muñoz, Francesc Molist, Raquel Quintanilla, Miguel Perez-Enciso, and Yulixaxis Ramayo-Caldas. kernInt: A kernel framework for integrating supervised and unsupervised analyses in spatio-temporal metagenomic datasets. *Frontiers in microbiology*, 12:60, 2021.
- Timothy W Randolph, Sen Zhao, Wade Copeland, Meredith Hullar, and Ali Shojaie. Kernel-penalized regression for analysis of microbiome data. *The annals of applied statistics*, 12(1):540, 2018.
- Albane Ruaud, Niklas Pfister, Ruth E. Leya, and Nicholas D. Youngbluta. Interpreting tree ensemble machine learning models with endor. *bioRxiv preprint bioRxiv: 2022.01.03.474763v1*, 2022. doi: <https://doi.org/10.1101/2022.01.03.474763>.
- W. Samek, G. Montavon, A. Vedaldi, L. K. Hansen, and K.-R. Müller. *Explainable AI: interpreting, explaining and visualizing deep learning*, volume 11700. Springer Nature, 2019.
- Isaac Jacob Schoenberg. Metric spaces and positive definite functions. *Transactions of the American Mathematical Society*, 44, 1938.
- B. Schölkopf, A. J. Smola, and F. Bach. *Learning with kernels: support vector machines, regularization, optimization, and beyond*. MIT press, 2002.
- Pixu Shi, Anru Zhang, and Hongzhe Li. Regression analysis for microbiome compositional data. *The Annals of Applied Statistics*, 10(2):1019 – 1040, 2016. doi: 10.1214/16-AOAS928. URL <https://doi.org/10.1214/16-AOAS928>.
- Léo Simpson, Patrick Combettes, and Christian Müller. c-lasso - a python package for constrained sparse and robust regression and classification. *Journal of Open Source Software*, 6:2844, 01 2021. doi: 10.21105/joss.02844.
- B. K. Sriperumbudur, K. Fukumizu, and G. Lanckriet. Universality, characteristic kernels and rkhs embedding of measures. *Journal of Machine Learning Research*, 12(7), 2011.

- B. D. Topçuoğlu, N. A. Lesniak, M. Ruffin IV, J. Wiens, and P. D. Schloss. A framework for effective application of machine learning to microbiome-based classification problems. *MBio*, 11(3):e00434–20, 2020.
- Flemming Topsøe. Jensen-Shannon divergence and norm-based measures of discrimination and variation. *preprint*, 2003.
- Michail Tsagris and Giorgos Athineou. *Compositional: Compositional Data Analysis*, 2021. URL <https://CRAN.R-project.org/package=Compositional>. R package version 4.5.
- Michail T Tsagris, Simon Preston, and Andrew TA Wood. A data-based power transformation for compositional data. *arXiv preprint arXiv:1106.1451*, 2011.
- Matthew CB Tsilimigras and Anthony A Fodor. Compositional data analysis of the microbiome: fundamentals, tools, and challenges. *Annals of epidemiology*, 26(5):330–335, 2016.
- Guido van Rossum and Fred L Drake. *Python 3 Reference Manual*. CreateSpace, 2009.
- James Howard Wells and Lynn R Williams. *Embeddings and extensions in analysis*, volume 84. Springer Science & Business Media, 2012.
- Ni Zhao, Jun Chen, Ian M. Carroll, Tamar Ringel-Kulka, Michael P. Epstein, Hua Zhou, Jin J. Zhou, Yehuda Ringel, Hongzhe Li, and Michael C. Wu. Testing in microbiome-profiling studies with mirkat, the microbiome regression-based kernel association test. *The American Journal of Human Genetics*, 96(5):797–807, 2015. ISSN 0002-9297. doi: <https://doi.org/10.1016/j.ajhg.2015.04.003>. URL <https://www.sciencedirect.com/science/article/pii/S0002929715001408>.
- Y.-H. Zhou and P. Gallins. A review and tutorial of machine learning methods for microbiome host trait prediction. *Frontiers in genetics*, page 579, 2019.